Molecular Therapy
Original Article

Ginseng-derived nanoparticles potentiate immune checkpoint antibody efficacy by reprogramming the cold tumor microenvironment

Xuan Han,[1] Qin Wei,[1] Yan Lv,[1] Ling Weng,[1] Haoying Huang,[1] Qingyun Wei,[1] Mengyuan Li,[2] Yujie Mao,[1] Di Hua,[1] Xueting Cai,[1] Meng Cao,[1] and Peng Cao[1,2,3]

[1]Affiliated Hospital of Integrated Traditional Chinese and Western Medicine, Nanjing University of Chinese Medicine, Nanjing, Jiangsu, China; [2]College of Pharmacy, Nanjing University of Chinese Medicine, 138 Xianlin Rd., Nanjing, Jiangsu 210023, China; [3]Collaborative Innovation Centre for Cancer Medicine, Nanjing Medical University, Nanjing, Jiangsu, China

Cold tumor microenvironment (TME) marked with low effector T cell infiltration leads to weak response to immune checkpoint inhibitor (ICI) treatment. Thus, switching cold to hot TME is critical to improve potent ICI therapy. Previously, we reported extracellular vesicle (EV)-like ginseng-derived nanoparticles (GDNPs) that were isolated from *Panax ginseng C.A. Mey* and can alter M2 polarization to delay the hot tumor B16F10 progression. However, the cold tumor is more common and challenging in the real world. Here, we explored a combinatorial strategy with both GDNPs and PD-1 (programmed cell death protein-1) monoclonal antibody (mAb), which exhibited the ability to alter cold TME and subsequently induce a durable systemic anti-tumor immunity in multiple murine tumor models. GDNPs enhanced PD-1 mAb anti-tumor efficacy in activating tumor-infiltrated T lymphocytes. Our results demonstrated that GDNPs could reprogram tumor-associated macrophages (TAMs) to increase CCL5 and CXCL9 secretion for recruiting $CD8^+$ T cells into the tumor bed, which have the synergism to PD-1 mAb therapy with no detected systemic toxicity. *In situ* activation of TAMs by GDNPs may broadly serve as a facile platform to modulate the suppressive cold TME and optimize the PD-1 mAb immunotherapy in future clinical application.

INTRODUCTION

By inactivating inhibitory immune receptors (immune checkpoints), immune checkpoint inhibitor (ICI) therapies have greatly expanded the landscape of carcinoma treatment.[1,2] Among ICI therapies, monoclonal antibodies (mAbs) targeting programmed cell death protein-1 (PD-1) or its ligand PD-L1 have become popular inhibitors that can activate tumor-infiltrated T lymphocytes and induce an anti-tumor immune response. Currently, many clinical trials on PD-1/PD-L1 therapies have shown promising therapeutic outcomes in multiple types of cancer.[3] However, there has been a relatively low overall response rate in a large proportion of patients who undergo ICI treatments.[1] T cell infiltration into tumors may be the primary factor for effective ICI treatments, and tumors with high T cell infiltration are defined as "hot" or "T cell-inflamed" tumors. When tumors per se lack T cell infiltration, or there is a paucity, they are characterized as "cold" or "non-inflamed" tumors.[4–6] Cold tumors typically do not respond well to ICI therapy, as in the case of colon, breast, and pancreatic cancers.[6,7] Therefore, boosting T cell infiltration into tumors is critical for improving the effects of ICI treatments.[8]

Tumor-associated macrophages (TAMs) play critical roles in supporting tumor progression, metastasis, and therapy resistance.[9,10] In the early stages of tumor formation, tumoricidal macrophages (M1-like, $CD206^{lo}CD86^{hi}$) are the main phenotype of TAMs. As the tumor microenvironment (TME) is modified to support tumor progression, tumor-supportive macrophages (M2-like, $CD206^{hi}CD86^{lo}$) represent the majority of TAMs in advanced tumor stage.[11] Thus, TAMs with plasticity can be further therapeutically exploited to reactivate anti-tumor properties.[12] Recent studies indicated that TAMs mediate the resistance of ICI or adoptive T cell immunotherapies.[13,14] So they have emerged as a target of immunotherapy. Notably, the expression of pro-tumor M2-like phenotype on TAMs is strongly correlated with poor prognosis.[15,16] Furthermore, TAM-targeting treatments in clinical trials and pre-clinical studies, such as colony-stimulating factor-1 receptor blockade,[17] interferon (IFN)-γ,[18] Toll-like receptor 7/8 (TLR7/8) agonists imiquimod,[15,19] and iron oxide nanoparticles,[20] indicated that reprogramming M2-like macrophage to M1 like or decreasing TAM tumor infiltration percentage is promising to effectively delay tumor progression. However, whether macrophage polarization by reprogramming macrophage could inflame the cold tumor immunophenotype to hot has not been reported.

Received 20 March 2021; accepted 20 August 2021;
https://doi.org/10.1016/j.ymthe.2021.08.028.

Correspondence: Peng Cao, College of Pharmacy, Nanjing University of Chinese Medicine, 138 Xianlin Rd., Nanjing, Jiangsu 210023, China.
E-mail: cao_peng@njucm.edu.cn
Correspondence: Meng Cao, Affiliated Hospital of Integrated Traditional Chinese and Western Medicine, Nanjing University of Chinese Medicine, Nanjing, Jiangsu, China.
E-mail: mcao1979@yahoo.com

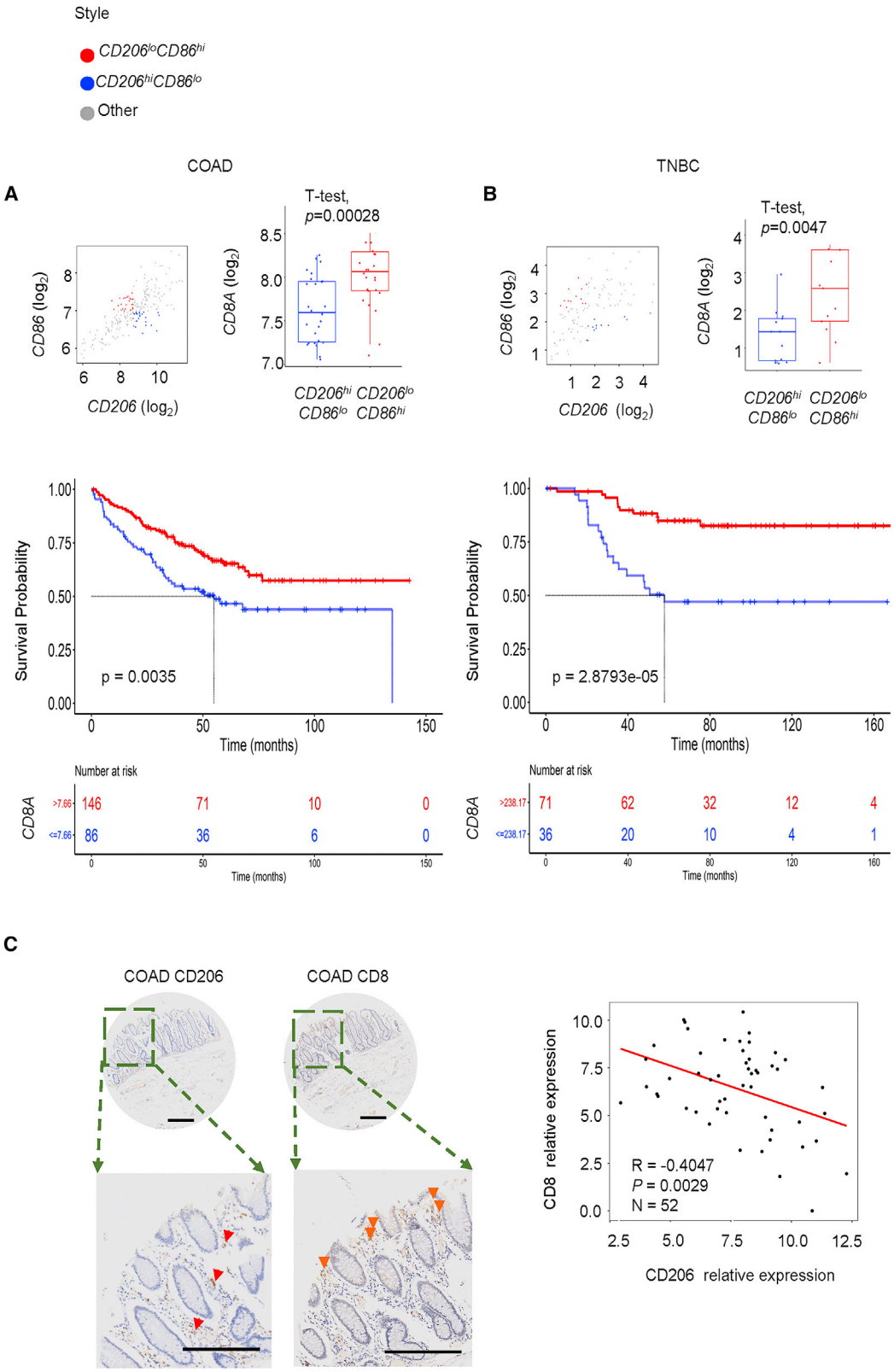

(legend on next page)

Our previous study demonstrated that ginseng-derived nanoparticles (GDNPs), isolated from fresh *Panax ginseng C.A. Mey*, induce macrophage polarization to the tumoricidal phenotype through the TLR4/myeloid differentiation antigen 88 (Myd88) signaling pathway.[21] We found that GDNPs monotherapy significantly suppressed B16-F10 tumor growth. Moreover, GDNPs increased $CD8^+$ T/regulatory T cells (Tregs) ratio in TME *in vivo* and promoted $CD8^+$ T lymphocyte proliferation *in vitro*. As GDNPs showed potential to reverse cold TME to hot, we hypothesized that GDNPs could be an auxiliary factor for ICI therapy.

In this study, we explored whether GDNPs combined with PD-1 blockade could alter the pro-tumor environment to an anti-tumor environment, initiated by polarizing M2-like to M1-like TAMs. The results demonstrated that, compared with T cells in the Vehicle group (immunoglobulin G [IgG] isotype), more T cells were recruited by TAM-derived chemokines to the TME after Combo (combinatorial) treatment. This Combo strategy aided conversion of the TME from cold to hot and further enhanced the anti-tumor efficacy of PD-1 mAb.

RESULTS

Immune checkpoint blockade response positively correlated with $CD206^{lo}CD86^{hi}CD8^{hi}$ status

The phenotype of TAMs is significantly correlated with patients' survival.[9] The high density of tumor-supportive (M2-like) macrophages in the TME may indicate poor prognosis.[22–24] To better explore the correlation between tumor-supportive ($CD206^{hi}CD86^{lo}$)/tumoricidal ($CD206^{lo}CD86^{hi}$) TAMs and tumor cytotoxic T lymphocytes (CTLs) in colon adenocarcinoma (COAD) and triple-negative breast cancers (TNBCs), gene transcript analyses using Gene Expression Omnibus (GEO) was performed. The results showed that *CD8A* gene expression is lower in patients with $CD206^{hi}CD86^{lo}$ than that of $CD206^{lo}$ $CD86^{hi}$ patients in both COAD and TNBC (Figure 1A, p = 0.00028, gene sets GEO: GSE17356 + GEO: GSE17357; Figure 1B, p = 0.0047, gene set GEO: GSE58812). Moreover, we found that patients with higher *CD8A* expression may indicate longer overall survival in both COAD and TNBC (Figure 1A, log rank test p = 0.0035, n = 355, best cut-off; Figure 1B, log rank test p = 2.8793e-05, n = 252, best cut-off). As CD206 expression could be treated as a surrogate for M2-like TAMs in tumors,[25] 52 clinical colorectal cancer samples were stained for CD206 and CD8A by immunohistochemistry. The results showed negative correlations between CD206 and CD8A in COAD tumor samples (Figure 1C; n = 52, R = −0.4047, p = 0.0029), which indicated that lower tumor-supportive macrophage infiltration in tumors is accompanied with higher $CD8^+$ T lymphocyte infiltration.

To mimic the ICI treatment efficiency in human cancer, we applied anti-PD-1 mAbs to multiple murine tumor models. As expected, PD-1 mAb alone significantly inhibited the growth of hot tumors such as B16-F10 murine melanoma[1,26] (Figures S1A and S1B), but mice bearing CT26 murine colon tumor and 4T1 murine breast tumor were resistant to PD-1 mAb treatment[27,28] (Figure S1B). Subsequently, we analyzed the TME in three murine models on day 21 following tumor inoculation by flow cytometry, and the results showed that a ratio of $F4/80^+/CD45^+$ is more than 10% in the 4T1 murine breast tumor, CT26 murine colon tumor, or B16-F10 murine melanoma model (Figure S1C). Moreover, to understand the association between ICI therapy resistance and TAMs characterization, correlations between a ratio of $CD8^+/CD45^+$ and tumor-supportive macrophages/TAMs ($CD206^+/F4/80^+$) were analyzed, and the results showed negative correlation in a CT26 murine colorectal cancer model, which were consistent with the results of gene expression trends in COAD (Figure S1D).

Therefore, we hypothesized that polarizing TAMs to the tumoricidal phenotype could effectively increase infiltration of $CD8^+$ T cells into the TME, which may inflame cold tumors to improve a response to ICI therapy.

Combo therapy of GDNPs and PD-1 mAb reverses TAMs polarization and effectively inhibits growth of multiple tumors

Our previous data demonstrated that GDNPs isolated from fresh ginseng root can effectively inhibit melanoma (hot tumor) progression by polarizing TAMs to M1-like macrophages.[21] Moreover, we found that the percentage of T cells in TME increased markedly. Based on these findings, we speculated that a GDNPs-induced increase in M1-like macrophages may improve immunosuppressive status in TME. Furthermore, GDNPs treatment can induce the activation of T cells to inflame cold tumors to hot tumors and enhance the efficacy of ICI. To clarify the efficacy of GDNPs in different tumor immunophenotypes, we prepared GDNPs as previously reported[21] and confirmed their characterization. The Nanosight tracking analysis showed that mean size GDNPs is around 200.4 nm (Figure S2A). Transmission electron microscopy (TEM) examination indicated that GDNPs are spherical in shape (Figure S2B). By developing a sensitive liquid chromatography-mass spectrometry (LC-MS) method, Ginsenoside Re contents of GDNPs in each batch were detected without significant changes (Figure S2C). Besides, the GDNPs macrophage targeting properties were reclarified as well (Figure S2D). Interestingly, a remarkable decrease in tumor growth in CT26 murine colon tumor and 4T1 murine breast tumor models with GDNPs treatment (Figure S1E) was observed. However, 5-time GDNPs treatment did not maintain the long-time survival of CT26 murine

Figure 1. CD8A and tumor-associated macrophages (TAMs) marker expression in clinical specimens from the Gene Expression Omnibus (GEO) cancer dataset and multiple tumor models

Samples across (A) colon adenocarcinoma (COAD) or (B) triple-negative breast cancer (TNBC) were divided into $CD206^{hi}CD86^{lo}$ and $CD206^{lo}CD86^{hi}$ using the median of all specimens (analyzed by t test, p = 0.00028 for COAD and p = 0.0047 for TNBC). Kaplan-Meier analyses of patients stratified by $CD8^{hi}$ versus $CD8^{lo}$ in (A) COAD or (B) TNBC (p = 0.0035 for COAD and p = 2.8793e-05 for TNBC). (C) Immunohistochemical staining of CD206 and CD8 in COAD samples (scale bars, 200 μm). Correlation analyses CD8 expression and CD206 expression in n = 52, p = 0.0029.

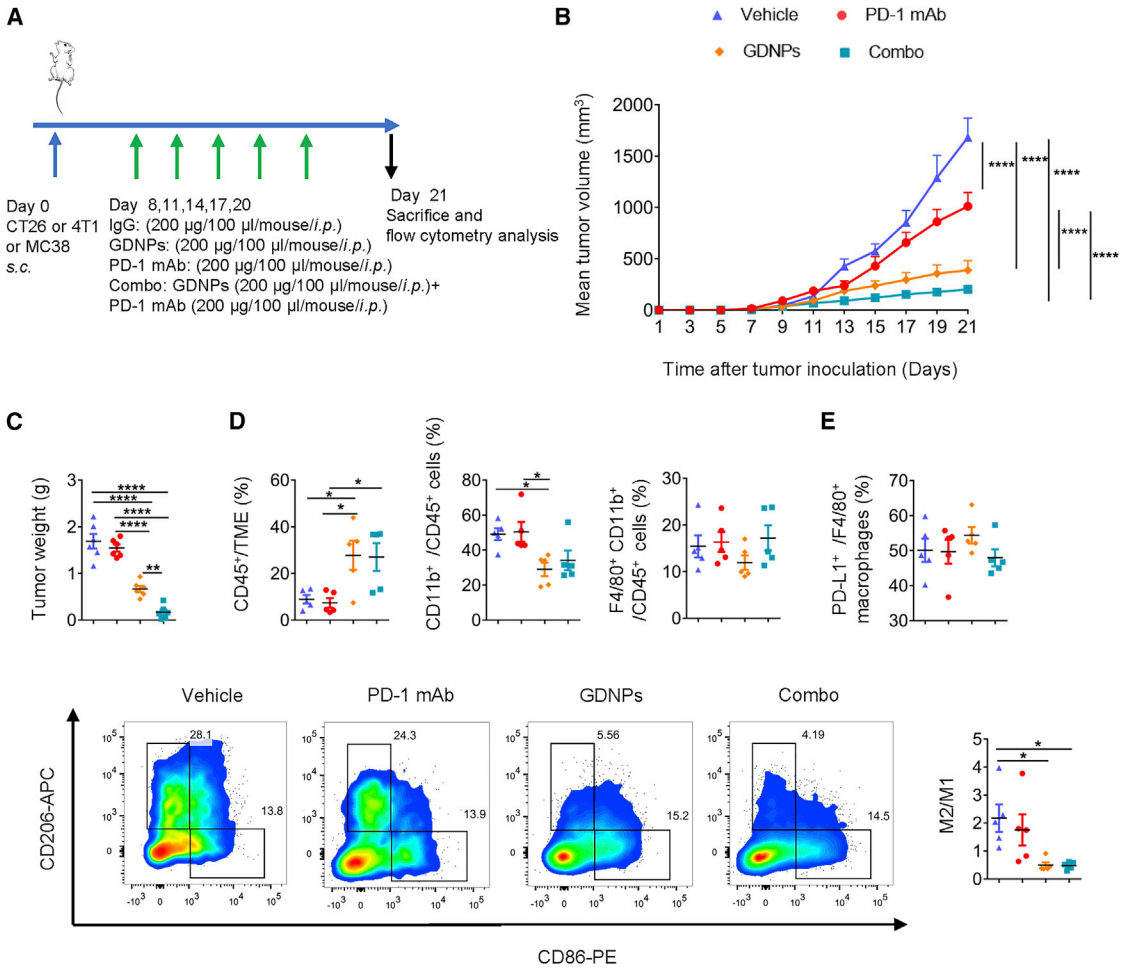

Figure 2. Combinatorial (Combo) therapy using GDNPs and PD-1 mAb elicits rejections of the CT26 murine colon tumor by polarizing M2-like macrophages to M1-like phenotype

(A) Time schedule for tumor implantation and drug treatment. (B) Tumor volume and (C) tumor weight for different treatment types, such as Vehicle, PD-1 mAb, GDNPs, or Combo treatment in CT26 murine colon tumor model (n = 6 for each group, one-way ANOVA or two-way ANOVA, **p < 0.01, ****p < 0.0001). (D) Ratio of $CD45^+$ in tumor microenvironment (TME), $CD11b^+CD45^+$ in immune cells, $F4/80^+CD11b^+$ in immune cells in the CT26 murine colon TME (n = 5 for each group, one-way ANOVA, *p < 0.05). (E) Representative fluorescence-activated cell sorting (FACS) plots and quantification of M2/M1. Percentage of $PD\text{-}L1^+/F4/80^+$ in TAMs. Representative flow cytometry picture for M2-TAM and M1-TAM (n = 5 for each group, one-way ANOVA, *p < 0.05).

tumor-bearing mice (clinical end point, tumor volume $\geq$ 2,000 mm^3; Figure S1F).

Thus, we evaluated whether the combination of PD-1 mAb with GDNPs could improve the anti-tumor response in cold tumors (Figure 2A). In the CT26 murine colon tumor model, the tumor progression in mice with Combo treatment was significantly delayed compared with that in the PD-1 mAb group and Vehicle group. Meanwhile, the GDNPs treatment was more efficient than Vehicle or PD-1 mAb treatments (Figure 2B). Consistently, the Combo group showed a much lower tumor weight (Figures 2C; Figure S3A) than Vehicle, PD-1 mAb, and GDNPs groups. Similar results were found in 4T1 murine breast tumor and MC38 murine colon tumor models (Figures S4A–S4D). Thus, we concluded that Combo treatment of PD-1 mAb and GDNPs enhanced anti-tumor efficiency in cold tumor models. In addition, monitoring mice weight (Figure S3B) and organ tissue histological staining (Figure S5) showed Combo treatment was tolerated without significant toxicity.

Further analyses of Tumor infiltrated lymphocytes (TILs) in TME were carried out on day 21 after tumor inoculation by flow cytometry. The results indicated that the percentage of $CD45^+$ immune cells increased 2- to 3-fold in tumors treated with GDNPs or Combo treatment than in those treated with PD-1 mAb in CT26-bearing mice (Figure 2D). In TILs, the percentage of myeloid cells in TME immune cells significantly decreased in the GDNPs group compared with that in the Vehicle or PD-1 mAb group (Figure 2D). The ratio of TAMs in

all TILs ($CD11b^+$ $F4/80^+/CD45^+$) did not differ in each group; however, GDNPs and Combo therapy decreased the M2/M1 ratio in tumors (Figures 2D and 2E). We also tested PD-$L1^+$ expression on TAMs and found no significant changes among different treatment groups (Figure 2E). Thus, these results suggested that re-polarizing of TAMs by GDNPs can enrich immune cells in the TME and improve the efficacy of ICIs in cold tumors.

Combination of GDNPs and PD-1 blockade promotes T lymphocyte infiltration and anti-tumor immune response

CTLs play a central role in killing tumor cells. The ratio of infiltrated $CD8^+$ T cells in tumors is the major difference that distinguishes cold tumors from hot ones.[24] As PD-1 mAb mainly targets CTLs, we validated the percentage of T cell infiltration and the protein level of cytotoxic cytokines in T lymphocytes. Analyses of the graft TME by flow cytometry showed an increase in T cell ($CD3^+/CD45^+$) infiltration in the CT26 murine colon cancer model after GDNPs or Combo treatment (Figure 3A). The ratio of $CD8^+/CD3^+$ increased in GDNP- and Combo-treated groups compared with that in the PD-1 mAb or Vehicle group (Figure 3B). We also analyzed CD8 protein expression in the CT26 murine colon tumor by immunohistochemistry (IHC), which showed the same trend as that in the flow cytometry analyses (Figure 3C).

CTLs are characterized by the secretion of IFN-γ, granzyme B, and tumor necrosis factor (TNF)-α, which kill tumor cells directly. In this study, the upregulation of IFN-γ and TNF-α was detected in tumor-infiltrated $CD8^+$ T cells from the CT26 murine graft colon tumor in the Combo group (Figures 3D and 3E). Meanwhile, $CD8^+$ T lymphocytes showed higher expression of $Ki67^+$ in the Combo-treated group compared with that in the PD-1 mAb/Vehicle group, which showed higher proliferation ability of CTLs in the Combo group (Figure 3E). We next focused on the expression of co-inhibitory molecules on T cells. For $CD8^+$ T cells, the lower expression of T cell Ig mucin domain-3 (TIM3; Figure S6A), inducible co-stimulator (ICOS; Figure S6B), and PD-1 (Figure S6C) was observed in the CT26 murine colon tumor with Combo treatment. These results indicated that combining GDNPs with PD-1 mAb therapy could induce $CD8^+$ T cell activation in the TME.

In addition, we found a higher T helper 1 cells (Th1)/Treg ratio (Figure 3G) and upregulated expression of granzyme B^+, IFN-γ^+, and TNF-α^+ $CD4^+$ T lymphocytes in tumors in the Combo group as compared to that of Vehicle-treated mice. Besides, the improved percentages of IFN-γ^+ and TNF-α^+ $CD4^+$ T lymphocytes were detected in the Combo group rather than those in the PD-1 mAb group. These results suggested that more $CD4^+$ T cells were differentiated into Th1 cells in the Combo-treated TME (Figures 3F and 3G). Besides, the Milliplex Luminex assay was performed to clarify the cytokine changes in the plasma in Combo treatment. Results showed that the concentrations of interleukin (IL)-2 and IL-12 p40 strongly increased in plasma under Combo treatment. Although the IL-12 p70 concentration showed no significant changes, the data are in the same trend as IL-2 (Figure S3C).

Finally, to validate the importance of $CD8^+$ and $CD4^+$ T lymphocytes in activating anti-tumor effects in Combo treatment, $CD8^+$ and $CD4^+$ T lymphocytes were independently ablated in CT26 murine colon tumor-bearing mice (Figure 4A). The depletion efficiency was confirmed in peripheral blood before Combo or Vehicle treatment by flow cytometry (Figures S7A and S7C). The results indicated that $CD8^+$ or $CD4^+$ T lymphocyte depletion reduced the Combo tumoricidal efficiency (Figures 4B and 4C; Figures S7B and S7D). Thus, these results are consistent with our hypothesis that $CD4^+$ and $CD8^+$ T lymphocytes play crucial roles in achieving efficacy with the Combo treatment. Taken together, these findings suggest that anti-tumor efficacy of Combo therapy is T lymphocyte dependent.

Combo therapy enhances long-term antigen-specific anti-tumor memory and inhibits tumor metastasis

Of note, 40% of CT26-bearing mice in the Combo group were ethically survived for over 50 days with treatment administered only 14 days after tumor inoculation (Figure 5A). As the surviving mice in the Combo group were accompanied with complete regression of CT26 murine colon tumors after the first inoculation, it raised the question whether the mice can survive the relapse of the tumors. A rechallenge assay revealed that approximately 50% of mice in the pre-Combo-treated group overcame CT26 murine colon tumor recurrence (Figures 5B and 5C). However, tumor rejection was not observed in the 4T1 murine breast tumor in the same mice. The results further verified the specificity of anti-tumor immune response induced by Combo treatment.

To further investigate the latent changes in the long-term antigen-specific anti-tumor memory behind the encouraging results, we evaluated memory T cells in the spleen by flow cytometry. In the spleen, central memory T lymphocytes ($CD44^+$ $CD62L^+$) and effector memory T lymphocytes ($CD44^+$ $CD62L^-$) in both $CD4^+$ and $CD8^+$ populations significantly increased in pre-Combo-treated survivors compared with that in tumor-bearing mice of the same age (Figure 5D). These results indicate that Combo treatment may elicit a durable anti-tumor immune memory.

As tumor metastasis highly affects the mobility and mortality of patients, we established a 4T1-Luc murine breast cancer lung metastasis model (Figure S8A). A significant reduction in tumor nodules in the lungs of the mice was observed with Combo treatment compared with that for treatment with PD-1 mAb alone (Figure S8B). Moreover, bioluminescent signals were also analyzed to assess lung metastasis. We found that Combo treatment decreased the luminescence in lungs of tumor-bearing mice (Figure S8C). These results indicate GDNPs combined with PD-1 mAb may activate the immune system to better depress tumor metastasis.

GDNPs elicited M2-like macrophage-secreting chemokines for T cell chemotaxis *in vitro*

Mounting evidence showed that GDNPs combined with PD-1 mAb optimized the TME by increasing TIL infiltration, which successfully

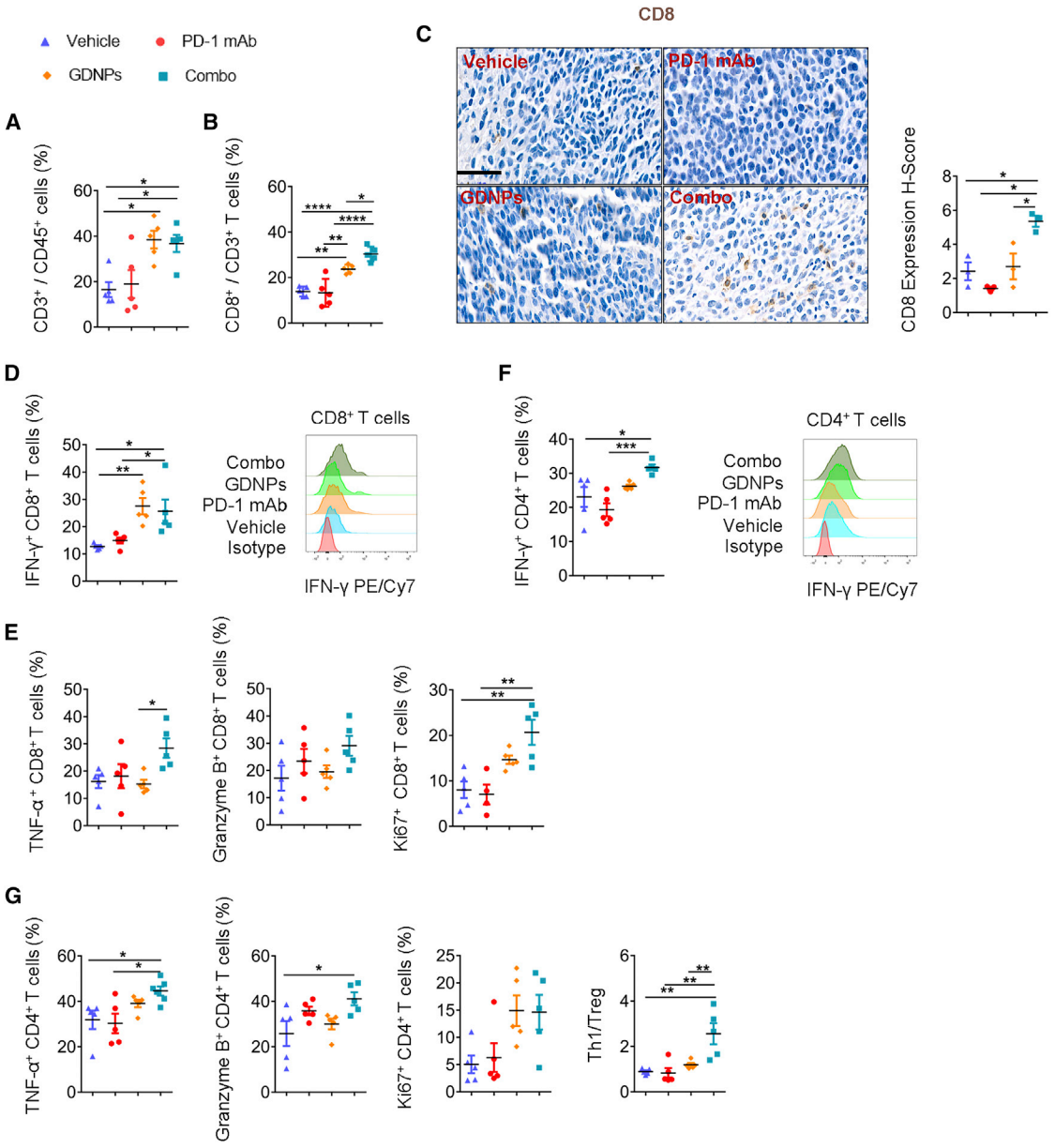

Figure 3. Combo treatment can activate tumor-infiltrated T lymphocytes

Ratio of different T cell phenotypes and T cell-related functional analyses in CT26 murine colon TME by FACS. (A) Ratio of $CD3^+$ in $CD45^+$ cells (n = 5 for each group, one-way ANOVA, *p < 0.05). (B) Ratio of $CD8^+$ in $CD3^+$ T cells (n = 5 for each group, *p < 0.05. **p < 0.01, ****p < 0.0001). (C) Representative pictures of CD8 IHC staining in TME and the quantification of the H-score of IHC staining for CD8 in CT26 murine colon tumor samples (scale bar, 50 μm; n = 3 for each group, *p < 0.05). (D) Quantification of IFN-γ^+ $CD8^+$ T cells and representative FACS histograms (n = 5 for each group, *p < 0.05, **p < 0.01). (E) Quantification of TNF-α^+ $CD4^+$ T cells, granzyme B^+ $CD8^+$ T cells, and $Ki67^+$ $CD4^+$ T cells (n = 5 for each group, *p < 0.05, **p < 0.01). (F) Quantification of IFN-γ^+ $CD4^+$ T cells and representative FACS histograms (n = 5 for each group, *p < 0.05, **p < 0.01). (G) Ratio of TNF-α^+ $CD4^+$ T cell, granzyme B^+ $CD4^+$ T cell, $Ki67^+$ $CD4^+$ T cell, and Th1/Treg (n = 5 for each group, *p < 0.05, **p < 0.01). Data are presented as mean ± SEM and analyzed by one-way ANOVA.

converted cold tumors to hot. This led us to explore how GDNPs-treated macrophages enhance T cell infiltration in the TME. To further clarify whether CTLs were recruited under GDNPs-treated bone marrow-derived macrophages (BMDMs) or not, 1,1'-dioctadecyl-3,3,3',3'-tetramethylindocarbocyanine perchlorate (DiI)-stained $CD8^+$ T cells ($CD8^+$ T microbeads isolated from spleen) were intravenously (i.v.) injected into tumor-bearing mice. The immunofluorescence staining data showed that GDNPs treatment recruited more $CD8^+$ T cells in the tumors than the phosphate-buffered saline (PBS) treatment group (Figure 6A).

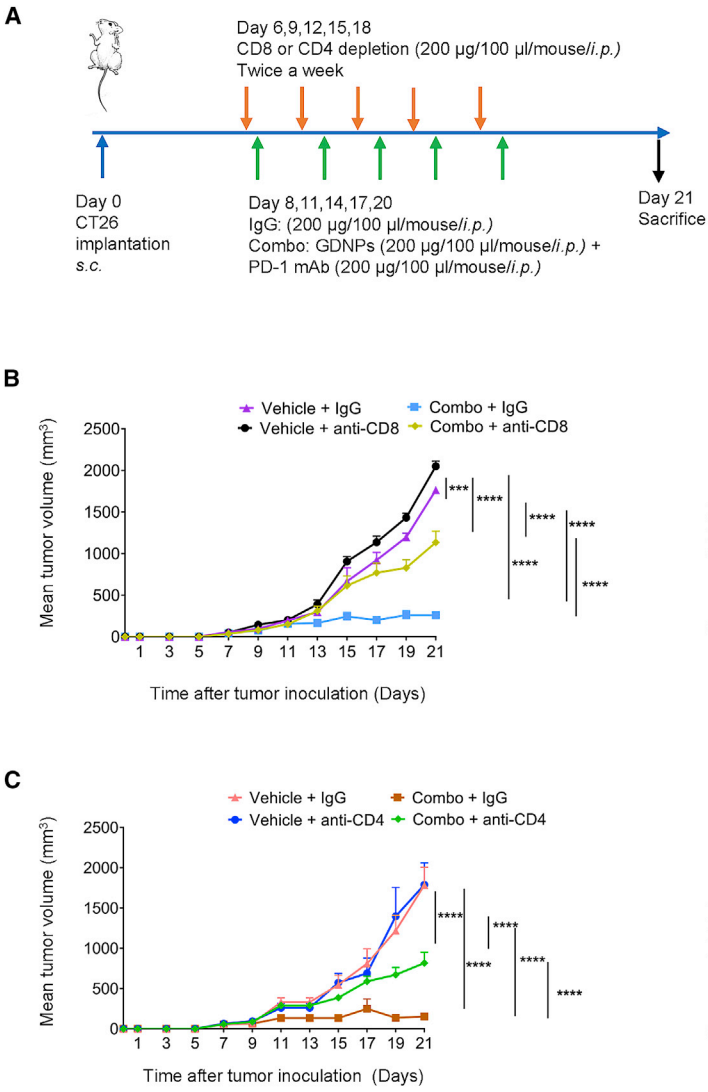

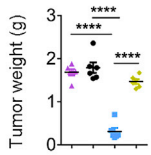

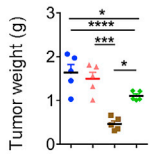

Figure 4. CD4⁺ T and CD8 ⁺ T lymphocytes play important roles in Combo treatment

(A) Paradigm of tumor implantation, $CD4^+$ or $CD8^+$ depletion, and drug treatment time schedule in CT26 murine colon cancer model. (B) Tumor volume and weight of Vehicle + IgG, Combo + IgG, Vehicle + anti-CD8, and Combo + anti-CD8 four groups (n = 6 for each group, ***p < 0.001, ****p < 0.0001). (C) Tumor volume and weight of Vehicle + IgG, Combo + IgG, Vehicle + anti-CD4, and Combo + anti-CD4 four groups (n = 5 for each group, *p < 0.05, ***p < 0.001, ****p < 0.0001). Data are presented as mean ± SEM and analyzed using one-way ANOVA or two-way ANOVA.

The $CD8^+$ T cell infiltration always has been measured by *Cd8a* transcript expression level in tumor tissue, and chemokines have been clarified to regulate immune cell trafficking and tumor development. Therefore, we selected *Cd8a* as a gene marker for quantifying chemokine-associated genes. We found that *Cd8a* expression significantly correlated to *Ccl5*, *Cxcl9*, *Cxcl10*, and *Cxcl13* high expression in COAD and TNBC across The Cancer Genome Atlas (TCGA) data (Figure 6B). Thus, we performed whole transcriptome RNA sequencing (RNA-seq) of M2-BMDMs with or without GDNPs *in vitro*, and the gene differential expression analyses showed significantly higher pro-inflammatory cytokines and chemokines, such as *Ccl2*, *Ccl3*, *Ccl5*, *Cxcl9*, and *Cxcl10* genes in the GDNP-treated group (Figure 6C). Based on the RNA-seq results and bioinformatic analyses, real-time polymerase chain reaction (PCR) for chemokines was performed. Our results confirmed the significantly increased expression of *Ccl5* and *Cxcl9* transcriptomes in M2-like macrophages with GDNPs treatment (Figure 6D). Based on the chemokine sequencing results,[21] we further analyzed the secretion of CCL5 and CXCL9 in culture media of M2-BMDMs and M2-BMDMs with GDNPs. Our findings confirmed that GDNPs treatment markedly increased M2-BMDMs secretion of CCL5 and CXCL9 (Figure 6E). To further examine the importance of GDNPs-treated TAMs in $CD8^+$ T lymphocyte chemotaxis, CCL5 and CXCL9 were inhibited using neutralizing antibodies in the culture media of TAMs under Combo treatment. The results showed a marked decrease of migrating T lymphocytes with the CCL5 and CXCL9 neutralization antibodies (Figure 6F). These findings indicated that TAMs under GDNPs treatment may promote more CCL5 and CXCL9 secretion to recruit T lymphocytes.

GDNPs facilitated TAM-derived CCL5 and CXCL9 secretion to recruit T lymphocytes *in vivo*

We analyzed the changes in chemokines secreted by TAMs in different treatment groups in CT26 murine colon cancer model. 2 weeks after CT26 colon tumor cell subcutaneous inoculation, we found that the expression of CCL5 (Figure 7A) and CXCL9 (Figure 7B) markedly increased in TAMs in the Combo group, and $CXCL9^+/F4/80^+$ significantly increased in the GDNPs group.

As the gene transcript of CXCL9 and CXCR3, CCL5 and CCR5 showed positive correlations in both COAD and BRCA, two tumor types (Figure S9),[29] we investigated CCL5 and CXCL9 receptors, CCR5 and CXCR3 expression on T lymphocytes in tumors by flow cytometry. Flow cytometry analyses indicated that $CCR5^+/CD8^+$ and $CCR5^+/CD4^+$ were found to significantly increase with Combo treatment in tumor samples (Figure 7C). These results indicated that increased chemokines from TAMs and chemokine receptors on T cells could be the causes of increased T lymphocyte infiltration.

Moreover, we found that higher CCL5 and CXCL9 expression in COAD and TNBC patients indicated longer overall survival, using

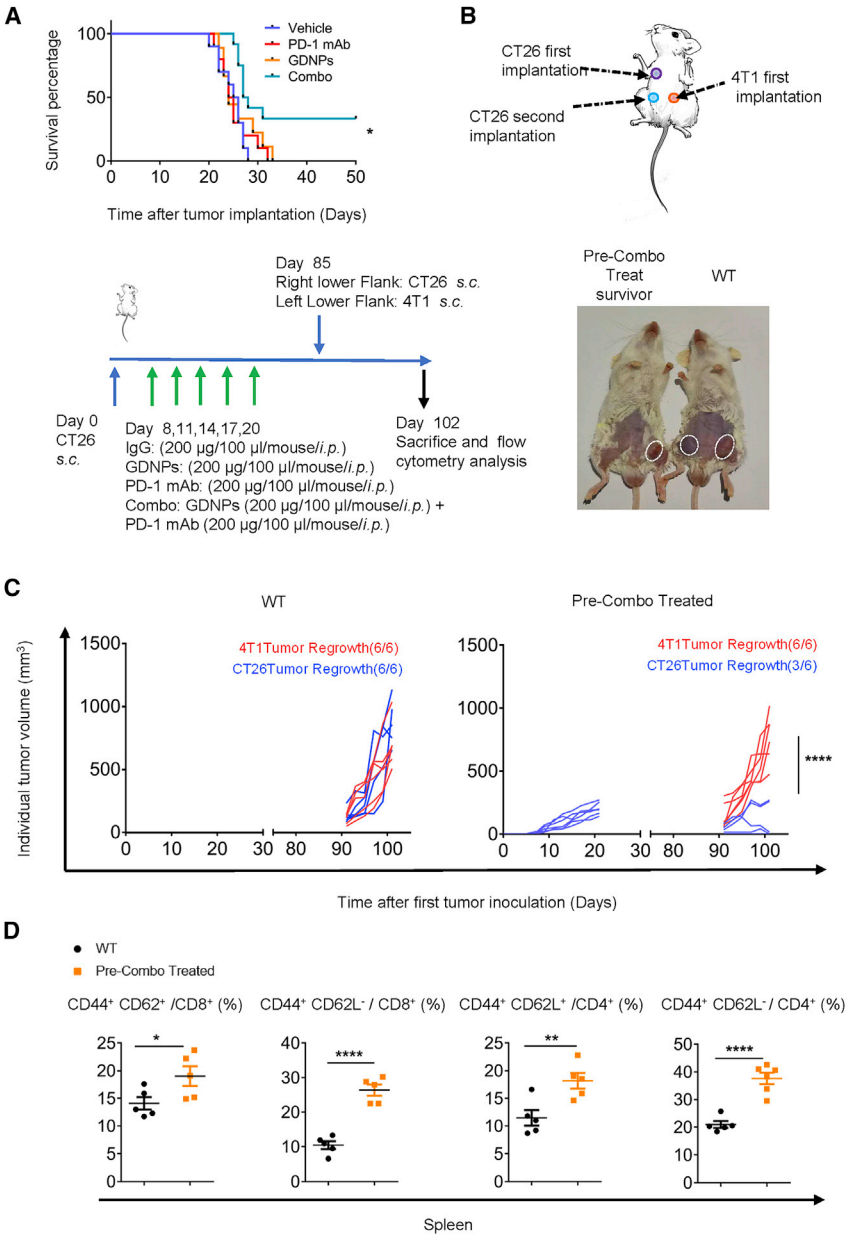

Figure 5. GDNPs combined with PD-1 mAb therapy enhance long-term antigen-specific anti-tumor memory

(A) Survival curves for Vehicle, PD-1 mAb, GDNPs, and Combo groups in the CT26 murine colon tumor model (n = 10 for each group, p = 0.0132). (B) Paradigm of tumor re-challenge assay and time schedule. (C) Quantification of tumor volumes for tumor rechallenge assay. Representative pictures for tumor-bearing mice (n = 6 for each group, ****p < 0.0001). (D) Quantification of $CD44^+$ $CD62L^+$ and $CD44^+$ $CD62L^-$ for $CD4^+$ or $CD8^+$ T cells in the spleen of wild-type (WT) or Combo pre-treated mice (n = 5 for each group, *p < 0.05, **p < 0.01, ****p < 0.0001). Data are presented as mean ± SEM and analyzed using two-way ANOVA, Student's t test, or log rank (Mantel-Cox) test.

TCGA and GEO datasets (Figure 7D). Taken together, GDNPs increased TAM-derived CCL5 and CXCL9 secretion for further T lymphocytes recruitment *in vivo* and were more efficient with PD-1 mAb treatment in cold tumors. In addition, we deleted the macrophage *in vivo* in the Combo-treated group using clodronate liposome (CL) (Figure S10A). Macrophage depletion efficiency by CL was confirmed by flow cytometry in peripheral blood (Figure S7E). The results showed a reverse of tumor decrease after in vivo macrophage deletion in Combo treatment (Figure S7F), and there was a reduction in CCL5 or CXCL9 in the tumor suspension in the Combo + CL group (Figure S10A), which verified the important roles of CCL5 and CXCL9 in a Combo-induced tumor decrease. Then, CD8 infiltration in tumors were verified by immunofluorescence simultaneously. The statistical results showed that CD8 infiltration significantly decreased in the Combo + CL group compared with the Combo group (Figure S10B). Thus, we confirmed that GDNPs activated macrophages to initiate the CD8+ T cell infiltration in TME. Besides, we neutralized the CCL5 and CXCL9 in the CT26 murine colorectal cancer model in vivo; the results showed that both αCCL5 and αCXCL9 significantly weakened the Combo-induced tumor depression (Figure S11A).

DISCUSSION

Among cancer immunotherapies, ICI treatment has yielded remarkable clinical benefits to many cancer patients. However, a large proportion of patients are refractory to PD-1/PD-L1 blockade treatment due to the paucity of tumor T cell infiltration that characterizes cold tumors. Thus, boosting T cell infiltration in tumors is critical for improving ICI treatment. Studies have reported many optional therapies for cold tumors, for example, radiotherapy, chemotherapy, targeted therapies, DNA repair-based therapy, adoptive cell therapy, oncolytic therapy, vaccine-based therapy, and T cell immunomodulators.[8,30,31] However, those therapies have not been clearly verified to effectively change cold tumors to hot. Thus, employing ICI-related Combo treatment to improve therapy efficacy raises great interest in translational medicine of related research.[7,32]

For most tumor types, especially cold tumors, TAMs are the major immune cells in the TME, and a high percentage of M2-like TAMs infiltration indicates poor clinical prognosis. Thus, targeting of TAMs using pan-therapy strategies, including targeting polarization signaling pathway and TAMs phagocytosis, has gained great interest.[9,33] Many studies have published various strategies for

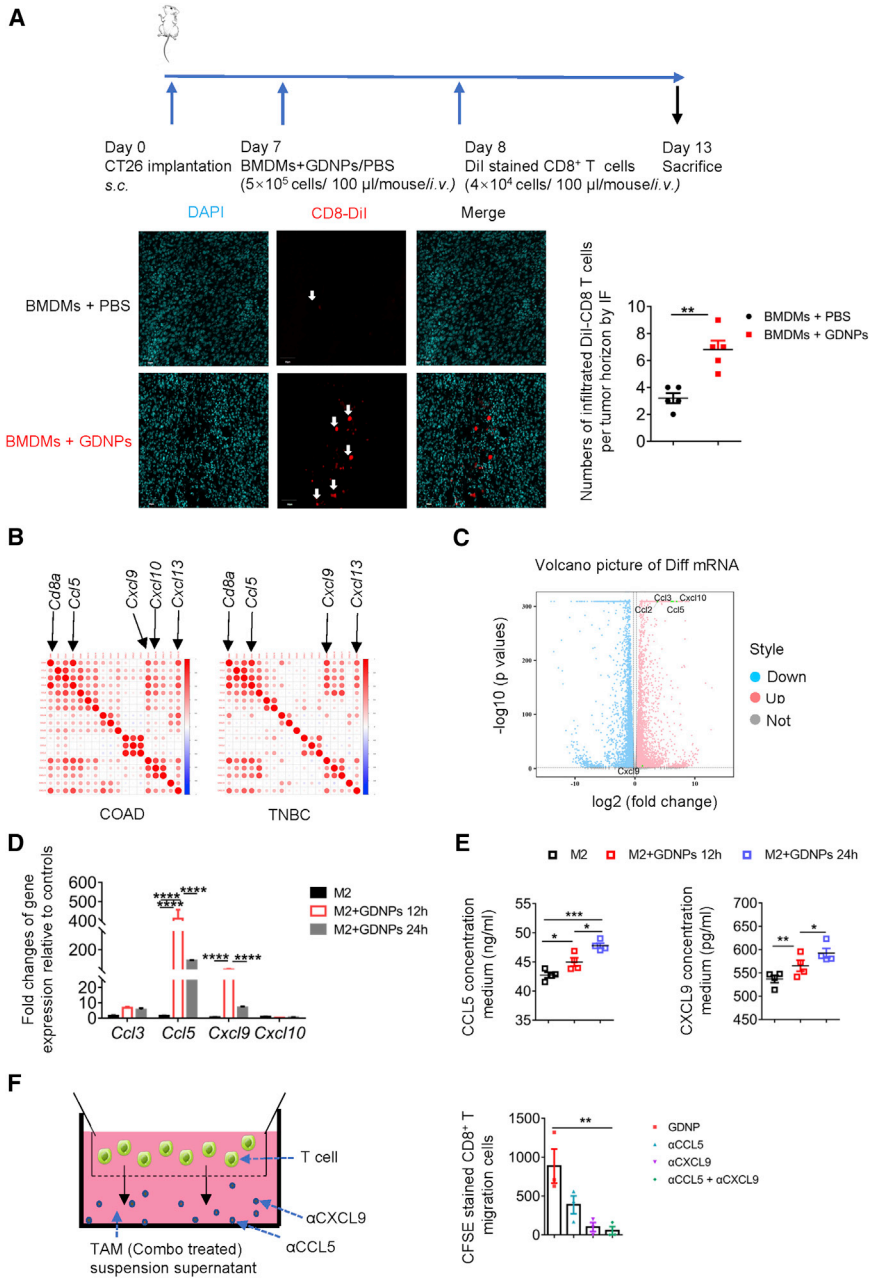

Figure 6. GDNPs may elicit macrophages to secrete chemokines for T cell chemotaxis

(A) $CD8^+$ T trafficking and biodistribution of DiI-labeled $CD8^+$ T lymphocytes in CT26 murine colon tumor with BMDMs + PBS or BMDMs + GDNPs treatment administered intravenously (scale bar, 50 μm; n = 5 for each group, $^{**}p < 0.01$). (B) Bubble plots showing correlations between *Cd8a* and chemotactic gene-related transcripts in COAD and TNBC from TCGA cancer datasets. (C) Volcano plot showing upregulated chemotactic gene expression from results of RNA sequencing for M2-BMDMs + GDNPs or M2-BMDMs + PBS ($p < 0.05$, fold change (FC) > 1.2, three samples each group). (D) Relative gene expressions of Ccl3, Ccl5, Cxcl9, and Cxcl10 in M2 like-BMDMs or GDNPs-stimulated M2-BMDMs for 12 h/24 h by real-time PCR (n = 3–4 for each group, $^{****}p < 0.0001$). (E) CCL5 and CXCL9 concentration in the culture media of M2-BMDMs, GDNPs + M2-BMDMs for 12 h, and GDNPs + M2-BMDMs for 24 h by ELISA (n = 4 for each group, $^{*}p < 0.05$, $^{***}p < 0.001$). (F) Schematic diagram and quantification of chemotactic assay. CFSE-stained $CD8^+$ T cells migrated toward the supernatant from TAM culture media of the Combo group in the presence of anti-CCL5 and anti-CXCL9 neutralization by flow cytometry (n = 3 for each group, $^{**}p < 0.01$). For all panels, data are presented as mean ± SEM and analyzed using one-way ANOVA or Student's t test.

TAMs-M1 polarization in tumor therapy including extracellular vesicles (EVs).[20,34] Some reports have demonstrated that different EVs from others mammalian cells with high stability and high bioavailability are a promising candidate for drug delivery systems. Compared with mammalian cell-derived EVs[35] and artificial EVs, plant-derived EVs are more advantageous with respect to scale-up and non-toxicity.[36] Many studies have identified that multiple plant-derived EVs have biological properties of tissue and organ specificity and low immunogenicity and are easily mass produced.[37–39] GDNP, a plant-derived nanoparticle drug, is a discovery in the cutting-edge area of EV drug delivery, with many advantages similar to most of plant-derived nanoparticles. However, to data, GDNPs are the only reported fresh plant-derived EVs to cause TAMs polarization to the tumoricidal phenotype, and their high biosafety demonstrates that GDNPs could be safely used in combination with ICI.

By analyzing the transcript expression between *CD8* and *CD206^{hi}CD86^{lo}* in multiple human cold tumors, the results indicated that M1-like macrophage polarization may improve the cold TME by increasing CD8 infiltration and reversing cold tumors to hot. In this study, GDNPs combined with PD-1 mAb therapy inhibited tumor progression more efficiently in three different murine tumor models compared with PD-1 mAb treatment alone. The Combo treatment successfully altered macrophage polarization and overcame low $CD8^+$ T cell infiltration to improve the effects of anti-PD-1.

An activated immune system accompanied with immunological memory is necessary for resisting tumor relapse.[26,27] Besides, tumor metastasis plays an important role in patient mortality, as lung metastasis mostly occurs in advanced breast cancer progress.[40] The CT26 murine colon cancer rechallenge assay and 4T1-Luc murine breast cancer lung metastasis assay were performed, and the results

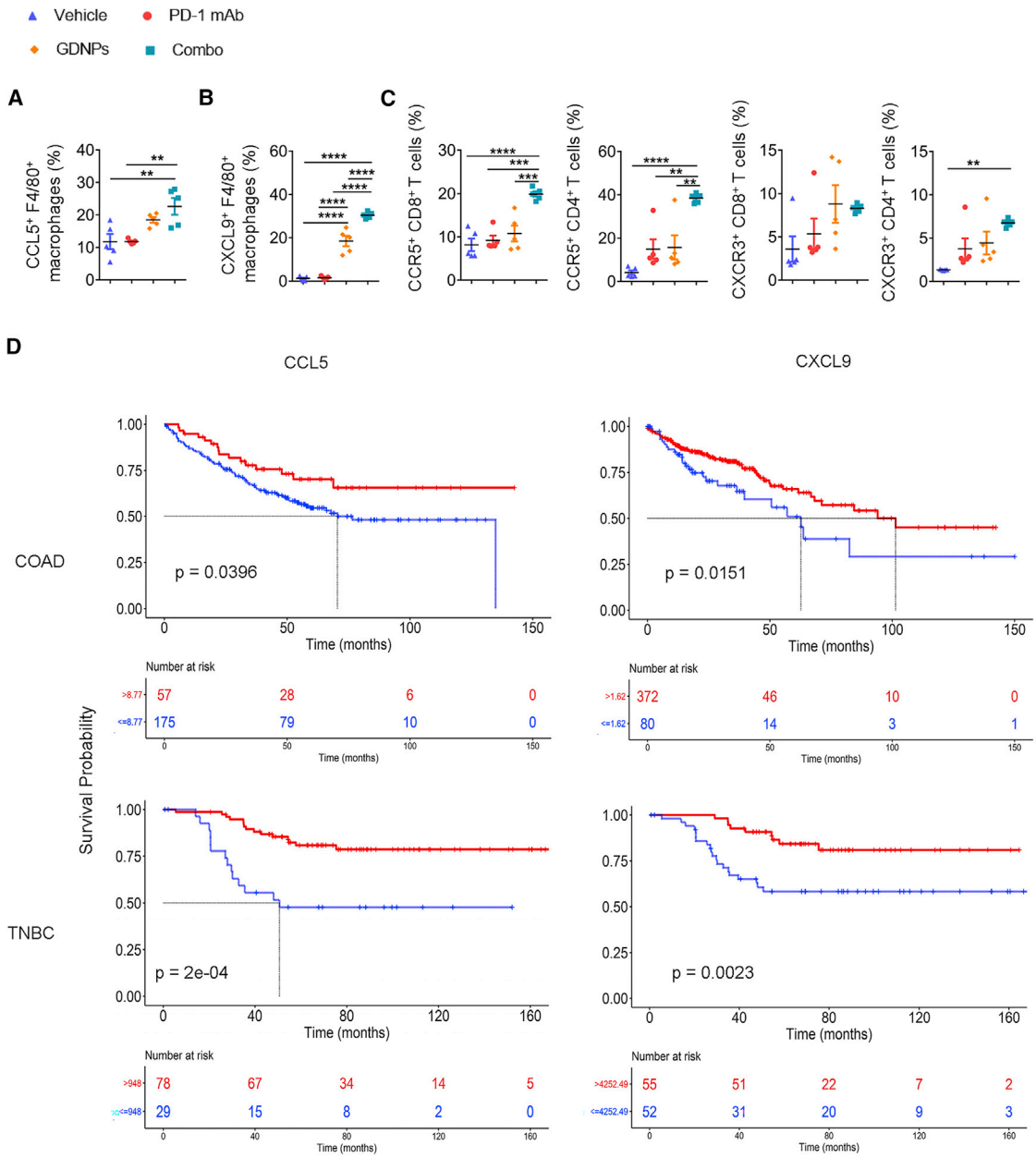

Figure 7. GDNPs combined with PD-1 mAb elicit TAM-secreting chemokines to change the TME

(A) Ratio of $CCL5^+/F4/80^+$ and (B) $CXCL9^+/F4/80^+$ in CT26 colon tumor model TME under Vehicle, PD-1 mAb, GDNPs, or Combo treatment (n = 5 for each group, $^{**}p < 0.01$, $^{****}p < 0.0001$). (C) Ratio of $CCR5^+/CD8^+$, $CXCR3^+/CD8^+$, $CCR5^+/CD4^+$, and $CXCR3^+/CD4^+$ in tumors with Vehicle, PD-1 mAb, GDNPs, or Combo treatment in CT26 murine colon tumor models (n = 5 for each group, $^{**}p < 0.01$, $^{***}p < 0.001$, $^{****}p < 0.0001$). Kaplan-Meier analyses for (D) COAD or TNBC datasets from GEO and TCGA were divided into two groups independently, stratified by CCL9 or CXCL5 median of all specimens (p = 0.04 for CCL5 in COAD, p = 0.015 for CXCL9 in COAD, p = 0.00018 for CCL5 in TNBC, p = 0.0023 for CXCL9 in TNBC). Data are presented as mean ± SEM and analyzed using one-way ANOVA or Kaplan-Meier analyses.

indicated that GDNPs combined with PD-1 mAb effectively activated the immune system, which helps to reduce tumor relapse and depress tumor lung metastasis foci formation.

To better illustrate the mechanism through which GDNPs-reprogrammed macrophages increased the ratio of T cells in the TME, multiple assays were performed. The results all supported that chemokines secreted by GDNP-polarized macrophages are the main cause of T cell tumor infiltration. Chemokines regulate the migration of leukocytes, and inducible chemokines increase at the inflamed site, which recruits activated leukocytes.[41,42] Indeed, chemokines such as CCL5, CXCL9, CXCL13, CXCL10, and CXCL16 have been reported

to recruit effector $CD8^+$ T cells in the tumors, resulting in an anti-carcinoma TME.[31,37,42–44] Our data indicated that CCL5 and CXCL9 induced by GDNPs polarized M1-like macrophages, contributing to the hot tumor immunophenotype establishing, which is consistent with previous reports.[45]

Whereas T lymphocyte recruitment-related chemokines increased in the TME, some chemokine receptors, such as CCR5 and CXCR3, are highly expressed in T lymphocytes as well, which are important for T lymphocyte infiltration in tumor beds. In our study, the increased T lymphocyte receptors CXCR3 and CCR5 enhanced CTL activation under Combo treatment. Although PD-1 mAb treatment alone led to a marked increase in CCR5 expression on $CD4^+$ T cells, it was not sufficient to change the cold tumor immunophenotype. The key role of CXCL9 that binds CXCR3 on T cells enhances recruitment of $CD4^+$ T cells and promotes the differentiation of inflammatory Th1 $CD4^+$ T cells as well. CCR5 and CXCR3 are known markers of activated T lymphocytes, especially Th1 cells, and their anti-tumor properties are well studied.[46–48] These results indicate that the Combo treatment can effectively transform cold tumors to hot by activating peripheral T lymphocytes.

Based on most of the anti-tumor immune indicators in this research, the results showed that the treatment efficacy of Combo was superior to GDNPs or PD-1 mAb alone. We speculated that it is because GDNPs reverse TME to make the PD-1 mAb treatment more effective, and PD-1 mAb blocked PD-1 function in TAMs in the Combo group, which is important to emancipate reprogrammed TAM anti-tumor efficacy.[49] Besides, our previous study indicated that ceramides, an important lipid component of GDNPs, polarized macrophages to the pro-inflamed phenotype by activating the TLR4-dependent signaling pathway.[50] Following TLR4 activation, Th1 proinflammatory cytokines such as TNF-α and IL-12p70 are highly secreted by macrophages.[51] In fact, Th1 activation is necessary for subsequent CTLs activation, which is important for T cell chemotaxis initiation.

Although the macrophage depletion effectively indicates the importance of CCL5 and CXCL9 *in vivo*, the results of the mean tumor volume in Combo + CL are significantly lower than the Vehicle group. Our previous research presented that granulocytes and dendric cells could phagocytose a small amount of GDNPs, which could be activated as well.[21] As the CL could only deplete 83% macrophages in this research (Figures S7E and S7F), and monocytes could differentiate into macrophages continuously,[10,52] there are still some macrophages that survived the CL treatment. In the future, we will continue to figure out the bioactivation for GDNPs on other immune cells. Besides, many studies have published that tumors with low tumor mutation burden (TMB) are accompanied with a low ICI treatment response rate.[53] As CT26 and MC38 murine tumor cells have been reported with a high TMB, and 4T1 has been recognized with a low TMB,[54,55] we hypothesized that GDNPs treatment could improve the PD-1 mAb efficacy in low TMB, and more research will be performed to verify the hypothesis in future.

Compared with other reported ICI-related Combo therapies, our GDNPs and ICI Combo therapy are the discovery of fresh plant-derived EVs, which are efficient in tumoricidal agents and lack obvious side effects. As the pharmaceutical content of GDNPs may have unintended reactions in tumors and other diseases, concrete steps are necessary to be taken. Moreover, the universality of GDNPs, combined with different ICI treatments in tumoricidal roles, and related clinical research are intensive further steps of this study.

MATERIALS AND METHODS

The ethics statement, patients' samples, study design, GDNPs preparation, RNA-seq analysis, and real-time PCR are presented in online Supplemental materials and methods.

Isolation of tumor-infiltrating cells and splenocytes

Mouse tumor tissues were sliced into 5 mm pieces and minced before using the Tumor Dissociation Kit (130096730, MACS) per the manufacturer's instructions.

The spleens were sliced into 5 mm pieces and passed through a 40-μm filter. After being mixed with red blood cell lysis buffer (C3702; Beyotime), the cells were resuspended in RPMI-1640 medium for future analyses.

After mice were anesthetized by isoflurane, 100 μL peripheral blood was collected from the mouse tail, and 5 mL red blood cell lysis buffer was added. After centrifugation at 300 × *g* for 5 min at 4°C, cells from peripheral blood were resuspended in RPMI-1640 medium for further analyses.

Flow cytometry of immune cells in the TME, splenocytes, and peripheral blood

Immune cells were isolated using Percoll (17-0891-09; GE Healthcare) from tumor cell suspension. These cells were incubated with CD16/32 (clone 93; BioLegend, San Diego, CA, USA) for 15 min on ice and then stained with various combinations of the following fluorochrome-conjugated antibodies at the appropriate dilutions for 30 min on ice: CD3-allophycocyanin (APC)/Cy7 (clone 145-2C11; BioLegend), CD8a-phycoerythrin (PE; clone 53-6.7; BioLegend), CD45-fluorescein isothiocyanate (FITC; clone 30-F11; BioLegend), CD11b-APC/Cy7 (clone M1/70; BioLegend), F4/80-PE/Cy7 (clone BM8; BioLegend), F4/80-BV421 (clone BM8; BioLegend), CD8a-APC (clone 53-6.7; BioLegend), CD4-APC (clone GK1.5; BioLegend), CD86-PE (clone PO3; BioLegend), CD206-APC (clone C068C2; BioLegend), CD25-APC (clone PC61.5; Invitrogen), CD4-PE/Cy7 (clone GK1.5; BioLegend), FVD450 (eflour 450; Invitrogen), FVD506 (eflour 506; Invitrogen), CD45-BV510 (clone 30-F11; BioLegend), CD62L-APC (clone MEL-14; BioLegend), CD44-PE (clone IM7; BioLegend), CCR5-APC (clone HIM-CCR5; Invitrogen), CXCR3-PE (clone CXCR3-173; BioLegend), TIM3-PE (clone 5D12/TIM-3; BD Pharmingen), ICOS-PE/Cy7 (clone 7E.17G9; Invitrogen), and PD-1-APC (clone 29F-1A12; BioLegend).

After cells were stained with surface markers, a Fixation/Permeabilization Kit (00-5123-43, 00-5223-56; Invitrogen) was used according to the manufacturer's instructions. Then, CCL5-PE (clone 2E9/CCL5; BioLegend), CXCL9-PE (clone MIG-2F5.5; BioLegend), Forkhead box protein P3 (FOXP3)-PE (clone FJK-16 s; Invitrogen), or Ki67-Peridinin Chlorophyll-Protein Complex (Percp)-Cy5.5 (clone B56; BD Biosciences) was diluted in the permeabilization buffer 10× (1:20) and incubated for 60 min on ice.

For T cell-derived anti-tumor cytokines, 2×10^6 splenocytes or TILs were incubated in RPMI-1640 medium with Cell Stimulation Cocktail Plus Protein Transport Inhibitors (500×) for 6 h. Then, the cells were stained with surface markers, fixed, and permeabilized using a Fixation/Permeabilization Kit, IFN-γ-PE/Cy7 (clone XMG1.2; BioLegend), granzyme B-FITC (clone NGZB; BioLegend), and TNF-α-BB700 (clone MP6-XT22; BD Horizon), which were diluent in the permeabilization buffer 10× (1:20) for 45 min.

Stained cells were analyzed on a FACSAria II Flow Cytometer; BD Biosciences) using BD FACSDiva software (BD Biosciences), and data were processed using FlowJo version 10 (BD Biosciences). Gating strategies were showed in Figure S12.

Preparation and polarization of mouse BMDMs

Mouse bone marrow was collected by flushing tibias and femurs of 9-week-old male BALB/c mice with cold PBS. After collection, red blood cells were lysed with the red blood cell lysis buffer (Beyotime), and the remaining cells were washed twice with PBS. To induce macrophage differentiation, the cells were cultured in DMEM with 10% fetal bovine serum and 20 ng/mL mouse macrophage colony-stimulating factor (M-CSF) (Bioworld Biotech, USA) for 6 days. On day 7, 20 ng/mL IL-4 (R&D Systems [R&D], USA) and 20 ng/mL IL-13 (R&D, USA) were added to polarize macrophages to the M2 phenotype macrophage for 48 h. The cells were prepared for real-time PCR.

Chemokine analyses

The supernatants of the M2 + GDNPs/PBS culture medium and the Combo-derived TAM culture medium were collected. Enzyme-linked immunosorbent assay (ELISA) was performed to examine the concentration of CCL5 and CXCL9 (ELISA kits were all from Mlbio, China), according to the manufacturer's instructions.

Chemotaxis assay

For $CD8^+$ T chemotaxis assay *in vivo*, CT26 murine colon cancer cell-bearing mice were i.v. administrated with 5×10^5 BMDMs under GDNPs or Vehicle pre-treated on day 7, followed by DiI-labeled 4×10^4 $CD8^+$ T cells i.v. on day 8. The mice were sacrificed, and the tumors were collected 5 days after $CD8^+$ T cell injection. Immunofluorescent assay was performed to analyze the tumor-infiltrated DiI-$CD8^+$ T lymphocytes.

For lymphocyte migration assay *in vitro*, the $CD8^+$ T MicroBeads Mouse Cell Isolation Kit (Miltenyi Biotec, USA) was used to obtain $CD8^+$ T lymphocytes from splenocytes. $CD8^+$ T lymphocytes were labeled for 3 min at 37°C in 5 mM carboxyfluorescein diacetate, succinimidyl ester (CFSE, Invitrogen, USA). Conditioned media (150 μL/well) of TAMs from Combo *in vitro* were loaded in the bottom as part of the Transwell migration chamber containing anti-CXCL9 1 μg/mL and anti-CCL5 1 μg/mL. CFSE-labeled $CD8^+$ T cells (3×10^4) were added to the top chamber in the DMEM culture media. Migration was evaluated by enumerating the number of migrated cells in the bottom chamber using fluorescence-activated cell sorting analyses after 24 h.

Bioinformatic analyses

Computations were performed with the R software system for statistics and figure generation.

For COAD and TNBC tumors, the multi-tumor gene expression microarray dataset from the Expression Project for Oncology (expO; http://www.intgen.org/; GEO: GSE17356 + GEO: GSE17357 COAD and GEO: GSE58812 TNBC) and survival data were analyzed using "survminer" R package.[56] TCGA (https://www.cancer.gov/about-nci/organization/ccg/research/structural-genomics/tcga) was used for multi-tumor chemokine gene expression data analyzed with the RTCGAToolbox R package.

For chemotaxis-related RNA transcription variation analyses between M2-BMDMs + PBS and M2-BMDMs + GDNPs, "ggplot2" R package was used; $p < 0.05$ and fold change = 1.2 were set as the criteria.

Statistical analyses

The results are expressed as the mean ± standard error of mean (SEM). All data were analyzed using GraphPad Prism 7.0 (GraphPad Software, USA) by unpaired Student's t test, one-way or two-way analyses of variance (ANOVA), and log rank (Mantel-Cox) test. $p < 0.05$ was considered statistically significant (*$p < 0.05$, **$p < 0.01$, ***$p < 0.001$, ****$p < 0.0001$).

SUPPLEMENTAL INFORMATION

Supplemental information can be found online at https://doi.org/10.1016/j.ymthe.2021.08.028.

ACKNOWLEDGMENTS

We thank Dr. Lixin Wang (Medical School, Southeast University) and Dr. Liwei Lu (The University of Hong Kong) for helpful discussion and critical reading of this manuscript. This work was supported by grants from the National Natural Science Foundation of China (no. 82125037, no. 81673945), Open Project of Chinese Materia Medica First-Class Discipline of Nanjing University of Chinese Medicine (no. 2020YLXK001), WINFAST Charity Foundation (RHKY20201215), Priority Academic Program Development of Jiangsu Higher Education Institutions (Integration of

Chinese and Western Medicine), and Technology Development Program of Traditional Chinese Medicine in Jiangsu Province (YB2020019).

AUTHOR CONTRIBUTIONS

The study was conceived, designed, and co-written by X.H., M.C., and P.C. The acquisition of data was performed by X.H., Q.W. (Qin Wei), Y.L., L.W., H.H., Y.M., M.L., and D.H. All authors contributed to the analyses of the data, discussed the results, edited the manuscript, and approved the final manuscript. Funding was obtained, and all studies were supervised by M.C. and P.C.

DECLARATION OF INTERESTS

The authors declare no competing interests.

REFERENCES

1. Gong, J., Chehrazi-Raffle, A., Reddi, S., and Salgia, R. (2018). Development of PD-1 and PD-L1 inhibitors as a form of cancer immunotherapy: a comprehensive review of registration trials and future considerations. J. Immunother. Cancer *6*, 8.
2. Zhu, X., and Lang, J. (2017). Soluble PD-1 and PD-L1: predictive and prognostic significance in cancer. Oncotarget *8*, 97671–97682.
3. Balar, A.V., and Weber, J.S. (2017). PD-1 and PD-L1 antibodies in cancer: current status and future directions. Cancer Immunol. Immunother. *66*, 551–564.
4. Duan, X., Chan, C., Han, W., Guo, N., Weichselbaum, R.R., and Lin, W. (2019). Immunostimulatory nanomedicines synergize with checkpoint blockade immunotherapy to eradicate colorectal tumors. Nat. Commun. *10*, 1899.
5. Oliveira, A.F., Bretes, L., and Furtado, I. (2019). Review of PD-1/PD-L1 Inhibitors in Metastatic dMMR/MSI-H Colorectal Cancer. Front. Oncol. *9*, 396.
6. Shin, D.S., Zaretsky, J.M., Escuin-Ordinas, H., Garcia-Diaz, A., Hu-Lieskovan, S., Kalbasi, A., Grasso, C.S., Hugo, W., Sandoval, S., Torrejon, D.Y., et al. (2017). Primary Resistance to PD-1 Blockade Mediated by JAK1/2 Mutations. Cancer Discov. *7*, 188–201.
7. Galon, J., and Bruni, D. (2019). Approaches to treat immune hot, altered and cold tumours with combination immunotherapies. Nat. Rev. Drug Discov. *18*, 197–218.
8. Zappasodi, R., Merghoub, T., and Wolchok, J.D. (2018). Emerging Concepts for Immune Checkpoint Blockade-Based Combination Therapies. Cancer Cell *33*, 581–598.
9. Cassetta, L., Fragkogianni, S., Sims, A.H., Swierczak, A., Forrester, L.M., Zhang, H., Soong, D.Y.H., Cotechini, T., Anur, P., Lin, E.Y., et al. (2019). Human Tumor-Associated Macrophage and Monocyte Transcriptional Landscapes Reveal Cancer-Specific Reprogramming, Biomarkers, and Therapeutic Targets. Cancer Cell *35*, 588–602.e10.
10. Ma, R.Y., Zhang, H., Li, X.F., Zhang, C.B., Selli, C., Tagliavini, G., Lam, A.D., Prost, S., Sims, A.H., Hu, H.Y., et al. (2020). Monocyte-derived macrophages promote breast cancer bone metastasis outgrowth. J. Exp. Med. *217*, e20191820.
11. Guerriero, J.L. (2018). Macrophages: The Road Less Traveled, Changing Anticancer Therapy. Trends Mol. Med. *24*, 472–489.
12. Cassetta, L., and Pollard, J.W. (2018). Targeting macrophages: therapeutic approaches in cancer. Nat. Rev. Drug Discov. *17*, 887–904.
13. Veldman, J., Visser, L., Berg, A.V.D., and Diepstra, A. (2020). Primary and acquired resistance mechanisms to immune checkpoint inhibition in Hodgkin lymphoma. Cancer Treat. Rev. *82*, 101931.
14. Peranzoni, E., Lemoine, J., Vimeux, L., Feuillet, V., Barrin, S., Kantari-Mimoun, C., Bercovici, N., Guérin, M., Biton, J., Ouakrim, H., et al. (2018). Macrophages impede CD8 T cells from reaching tumor cells and limit the efficacy of anti-PD-1 treatment. Proc. Natl. Acad. Sci. USA *115*, E4041–E4050.
15. Petty, A.J., and Yang, Y. (2017). Tumor-associated macrophages: implications in cancer immunotherapy. Immunotherapy *9*, 289–302.
16. Yang, M., McKay, D., Pollard, J.W., and Lewis, C.E. (2018). Diverse Functions of Macrophages in Different Tumor Microenvironments. Cancer Res. *78*, 5492–5503.
17. Shi, G., Yang, Q., Zhang, Y., Jiang, Q., Lin, Y., Yang, S., Wang, H., Cheng, L., Zhang, X., Li, Y., et al. (2019). Modulating the Tumor Microenvironment via Oncolytic Viruses and CSF-1R Inhibition Synergistically Enhances Anti-PD-1 Immunotherapy. Mol. Ther. *27*, 244–260.
18. Gao, Y., Yang, J., Cai, Y., Fu, S., Zhang, N., Fu, X., and Li, L. (2018). IFN-γ-mediated inhibition of lung cancer correlates with PD-L1 expression and is regulated by PI3K-AKT signaling. Int. J. Cancer *143*, 931–943.
19. Mullins, S.R., Vasilakos, J.P., Deschler, K., Grigsby, I., Gillis, P., John, J., Elder, M.J., Swales, J., Timosenko, E., Cooper, Z., et al. (2019). Intratumoral immunotherapy with TLR7/8 agonist MEDI9197 modulates the tumor microenvironment leading to enhanced activity when combined with other immunotherapies. J. Immunother. Cancer *7*, 244.
20. Zanganeh, S., Hutter, G., Spitler, R., Lenkov, O., Mahmoudi, M., Shaw, A., Pajarinen, J.S., Nejadnik, H., Goodman, S., Moseley, M., et al. (2016). Iron oxide nanoparticles inhibit tumour growth by inducing pro-inflammatory macrophage polarization in tumour tissues. Nat. Nanotechnol. *11*, 986–994.
21. Cao, M., Yan, H., Han, X., Weng, L., Wei, Q., Sun, X., Lu, W., Wei, Q., Ye, J., Cai, X., et al. (2019). Ginseng-derived nanoparticles alter macrophage polarization to inhibit melanoma growth. J. Immunother. Cancer *7*, 326.
22. Choi, J., Gyamfi, J., Jang, H., and Koo, J.S. (2018). The role of tumor-associated macrophage in breast cancer biology. Histol. Histopathol. *33*, 133–145.
23. La Fleur, L., Boura, V.F., Alexeyenko, A., Berglund, A., Pontén, V., Mattsson, J.S.M., Djureinovic, D., Persson, J., Brunnström, H., Isaksson, J., et al. (2018). Expression of scavenger receptor MARCO defines a targetable tumor-associated macrophage subset in non-small cell lung cancer. Int. J. Cancer *143*, 1741–1752.
24. Muhitch, J.B., Hoffend, N.C., Azabdaftari, G., Miller, A., Bshara, W., Morrison, C.D., Schwaab, T., and Abrams, S.I. (2019). Tumor-associated macrophage expression of interferon regulatory Factor-8 (IRF8) is a predictor of progression and patient survival in renal cell carcinoma. J. Immunother. Cancer *7*, 155.
25. Jaynes, J.M., Sable, R., Ronzetti, M., Bautista, W., Knotts, Z., Abisoye-Ogunniyan, A., Li, D., Calvo, R., Dashnyam, M., Singh, A., et al. (2020). Mannose receptor (CD206) activation in tumor-associated macrophages enhances adaptive and innate antitumor immune responses. Sci. Transl. Med. *12*, eaax6337.
26. De Henau, O., Rausch, M., Winkler, D., Campesato, L.F., Liu, C., Cymerman, D.H., Budhu, S., Ghosh, A., Pink, M., Tchaicha, J., et al. (2016). Overcoming resistance to checkpoint blockade therapy by targeting PI3Kγ in myeloid cells. Nature *539*, 443–447.
27. Ho, W.S., Wang, H., Maggio, D., Kovach, J.S., Zhang, Q., Song, Q., Marincola, F.M., Heiss, J.D., Gilbert, M.R., Lu, R., and Zhuang, Z. (2018). Pharmacologic inhibition of protein phosphatase-2A achieves durable immune-mediated antitumor activity when combined with PD-1 blockade. Nat. Commun. *9*, 2126.
28. Ma, H.S., Poudel, B., Torres, E.R., Sidhom, J.W., Robinson, T.M., Christmas, B., Scott, B., Cruz, K., Woolman, S., Wall, V.Z., et al. (2019). A CD40 Agonist and PD-1 Antagonist Antibody Reprogram the Microenvironment of Nonimmunogenic Tumors to Allow T-cell-Mediated Anticancer Activity. Cancer Immunol. Res. *7*, 428–442.
29. Li, T., Fu, J., Zeng, Z., Cohen, D., Li, J., Chen, Q., Li, B., and Liu, X.S. (2020). TIMER2.0 for analysis of tumor-infiltrating immune cells. Nucleic Acids Res. *48* (W1), W509–W514.
30. Trujillo, J.A., Sweis, R.F., Bao, R., and Luke, J.J. (2018). T Cell-Inflamed versus Non-T Cell-Inflamed Tumors: A Conceptual Framework for Cancer Immunotherapy Drug Development and Combination Therapy Selection. Cancer Immunol. Res. *6*, 990–1000.
31. Araujo, J.M., Gomez, A.C., Aguilar, A., Salgado, R., Balko, J.M., Bravo, L., Doimi, F., Bretel, D., Morante, Z., Flores, C., et al. (2018). Effect of CCL5 expression in the recruitment of immune cells in triple negative breast cancer. Sci. Rep. *8*, 4899.
32. Irvine, D.J., and Dane, E.L. (2020). Enhancing cancer immunotherapy with nanomedicine. Nat. Rev. Immunol. *20*, 321–334.
33. Cassetta, L., and Pollard, J.W. (2020). Tumor-associated macrophages. Curr. Biol. *30*, R246–R248.

34. Rao, L., Zhao, S.-K., Wen, C., Tian, R., Lin, L., Cai, B., Sun, Y., Kang, F., Yang, Z., He, L., et al. (2020). Activating Macrophage-Mediated Cancer Immunotherapy by Genetically Edited Nanoparticles. Adv. Mater. *32*, e2004853.

35. Yang, Y., Guo, Z., Chen, W., Wang, X., Cao, M., Han, X., Zhang, K, Teng, B, Cao, J, Wu, W., et al. (2021). M2 macrophage-derived exosomes promote angiogenesis and growth of pancreatic ductal adenocarcinoma by targeting E2F2. Mol. Ther. *29*, 1226–1238.

36. Woith, E., Fuhrmann, G., and Melzig, M.F. (2019). Extracellular Vesicles-Connecting Kingdoms. Int. J. Mol. Sci. *20*, 5695.

37. Wang, Q., Zhuang, X., Mu, J., Deng, Z.B., Jiang, H., Zhang, L., Xiang, X., Wang, B., Yan, J., Miller, D., and Zhang, H.G. (2013). Delivery of therapeutic agents by nanoparticles made of grapefruit-derived lipids. Nat. Commun. *4*, 1867.

38. Li, Z., Wang, H., Yin, H., Bennett, C., Zhang, H.G., and Guo, P. (2018). Arrowtail RNA for Ligand Display on Ginger Exosome-like Nanovesicles to Systemic Deliver siRNA for Cancer Suppression. Sci. Rep. *8*, 14644.

39. Yang, C., Zhang, M., and Merlin, D. (2018). Advances in Plant-derived Edible Nanoparticle-based lipid Nano-drug Delivery Systems as Therapeutic Nanomedicines. J. Mater. Chem. B Mater. Biol. Med. *6*, 1312–1321.

40. Kitamura, T., Qian, B.Z., Soong, D., Cassetta, L., Noy, R., Sugano, G., Kato, Y., Li, J., and Pollard, J.W. (2015). CCL2-induced chemokine cascade promotes breast cancer metastasis by enhancing retention of metastasis-associated macrophages. J. Exp. Med. *212*, 1043–1059.

41. Griffith, J.W., Sokol, C.L., and Luster, A.D. (2014). Chemokines and chemokine receptors: positioning cells for host defense and immunity. Annu. Rev. Immunol. *32*, 659–702.

42. Dangaj, D., Bruand, M., Grimm, A.J., Ronet, C., Barras, D., Duttagupta, P.A., Lanitis, E., Duraiswamy, J., Tanyi, J.L., Benencia, F., et al. (2019). Cooperation between Constitutive and Inducible Chemokines Enables T Cell Engraftment and Immune Attack in Solid Tumors. Cancer Cell *35*, 885–900.e10.

43. Zumwalt, T.J., Arnold, M., Goel, A., and Boland, C.R. (2015). Active secretion of CXCL10 and CCL5 from colorectal cancer microenvironments associates with GranzymeB+ CD8+ T-cell infiltration. Oncotarget *6*, 2981–2991.

44. Litchfield, K., Reading, J.L., Puttick, C., Thakkar, K., Abbosh, C., Bentham, R., Watkins, T.B.K., Rosenthal, R., Biswas, D., Rowan, A., et al. (2021). Meta-analysis of tumor- and T cell-intrinsic mechanisms of sensitization to checkpoint inhibition. Cell *184*, 596–614.e14.

45. Garrido-Martin, E.M., Mellows, T.W.P., Clarke, J., Ganesan, A.P., Wood, O., Cazaly, A., Seumois, G., Chee, S.J., Alzetani, A., King, E.V., et al. (2020). $M1^{hot}$ tumor-associated macrophages boost tissue-resident memory T cells infiltration and survival in human lung cancer. J. Immunother. Cancer *8*, e000778.

46. González-Martín, A., Gómez, L., Lustgarten, J., Mira, E., and Mañes, S. (2011). Maximal T cell-mediated antitumor responses rely upon CCR5 expression in both CD4(+) and CD8(+) T cells. Cancer Res. *71*, 5455–5466.

47. Mikucki, M.E., Fisher, D.T., Matsuzaki, J., Skitzki, J.J., Gaulin, N.B., Muhitch, J.B., Ku, A.W., Frelinger, J.G., Odunsi, K., Gajewski, T.F., et al. (2015). Non-redundant requirement for CXCR3 signalling during tumoricidal T-cell trafficking across tumour vascular checkpoints. Nat. Commun. *6*, 7458.

48. Fu, H., Ward, E.J., and Marelli-Berg, F.M. (2016). Mechanisms of T cell organotropism. Cell. Mol. Life Sci. *73*, 3009–3033.

49. Gordon, S.R., Maute, R.L., Dulken, B.W., Hutter, G., George, B.M., McCracken, M.N., Gupta, R., Tsai, J.M., Sinha, R., Corey, D., et al. (2017). PD-1 expression by tumour-associated macrophages inhibits phagocytosis and tumour immunity. Nature *545*, 495–499.

50. Fujiwara, N., Porcelli, S.A., Naka, T., Yano, I., Maeda, S., Kuwata, H., Akira, S., Uematsu, S., Takii, T., Ogura, H., and Kobayashi, K. (2013). Bacterial sphingophospholipids containing non-hydroxy fatty acid activate murine macrophages via Toll-like receptor 4 and stimulate bacterial clearance. Biochim. Biophys. Acta *1831*, 1177–1184.

51. Li, L., Jay, S.M., Wang, Y., Wu, S.W., and Xiao, Z. (2017). IL-12 stimulates CTLs to secrete exosomes capable of activating bystander $CD8^{+}$ T cells. Sci. Rep. *7*, 13365.

52. Qian, B.Z., Li, J., Zhang, H., Kitamura, T., Zhang, J., Campion, L.R., Kaiser, E.A., Snyder, L.A., and Pollard, J.W. (2011). CCL2 recruits inflammatory monocytes to facilitate breast-tumour metastasis. Nature *475*, 222–225.

53. Maleki Vareki, S. (2018). High and low mutational burden tumors versus immunologically hot and cold tumors and response to immune checkpoint inhibitors. J. Immunother. Cancer *6*, 157.

54. Fabian, K.P., Padget, M.R., Fujii, R., Schlom, J., and Hodge, J.W. (2021). Differential combination immunotherapy requirements for inflamed (warm) tumors versus T cell excluded (cool) tumors: engage, expand, enable, and evolve. J. Immunother. Cancer *9*, e001691.

55. Hos, B.J., Camps, M.G.M., van den Bulk, J., Tondini, E., van den Ende, T.C., Ruano, D., Franken, K., Janssen, G.M.C., Ru, A., Filippov, D.V., et al. (2019). Identification of a neo-epitope dominating endogenous CD8 T cell responses to MC-38 colorectal cancer. OncoImmunology *9*, 1673125.

56. Robinson, M.D., McCarthy, D.J., and Smyth, G.K. (2010). edgeR: a Bioconductor package for differential expression analysis of digital gene expression data. Bioinformatics *26*, 139–140.

YMTHE, Volume *30*

Supplemental Information

Ginseng-derived nanoparticles potentiate immune checkpoint antibody efficacy by reprogramming the cold tumor microenvironment

Xuan Han, Qin Wei, Yan Lv, Ling Weng, Haoying Huang, Qingyun Wei, Mengyuan Li, Yujie Mao, Di Hua, Xueting Cai, Meng Cao, and Peng Cao

Supplementary Materials and Methods

Mice，cell lines and ethics statement

Male and female 6-week-old BALB/c mice and C57BL6 mice were purchased from the Comparative Medicine Centre, Yangzhou University (Yangzhou, Jiangsu, China). All mice received access to food and water *ad libitum* and were housed in a temperature-controlled colony room with a 12/12-hour dark/light cycle. All animal experimental protocols were approved by the Institutional Animal Care and Use Committee of Nanjing University of Chinese Medicine.

The murine melanoma cell line B16-F10, murine colon cancer cell line CT26, murine luciferase expressed breast cancer cell line 4T1-Luc, and murine colon cancer cell line MC38 were purchased from the Institute of Biochemistry and Cell Biology, Academy of Science (Shanghai, China). Cells were cultured in Dulbecco's modified Eagle medium (DMEM) or Roswell Park Memorial Institute (RPMI) 1640, supplemented with 10% fetal bovine serum, 100 U/mL penicillin, and 100 mg/mL streptomycin (all from Thermo Fisher Scientific, USA). All cells were incubated at 37 °C in a humidified atmosphere with 5% CO_2.

Patient samples

Our study was conducted and archived colorectal carcinoma specimens (n = 52, 2020LWKYZ052) were collected according to the protocol of a human research ethics committee at Affiliated Hospital of Integrated Traditional Chinese and Western

Medicine (Nanjing, China) with patient's written formal consent. These patients have been followed over time.

Study design

This study was designed to characterize the efficiency of GDNPs combined with PD-1 mAb by analyzing samples from mice with tumors. Three murine tumor models (CT26, 4T1-luc, MC38) were selected to evaluate the combinatorial treatment efficiency. Six-week-old male mice were inoculated subcutaneously with 3×10^5 cells in the right upper flank ($n = 8$ per group, day 0). The first treatment was scheduled until the tumor was around 50 - 100 mm^3 on day 8. The control group received IgG (200 μg/100 μL/mouse/*i.p.*, clone 2AE, Bio X Cell, Lebanon, USA). PD-1 mAb (200 μg/100 μL/mouse/*i.p.*, clone BE0146, Bio X Cell, Lebanon, USA), GDNPs (200 μg/100 μL/mouse/*i.p.*) were injected intraperitoneally on day 8, 11, 14, 17 and 20 as Figure 2A demonstrated. The tumors were measured every other day with a caliper and the volume was calculated (length × $width^2/2$). Mice with no visible and touchable tumors on consecutive days were considered to have complementally regressed tumors. Mice were sacrificed when tumor volume was over 2000 mm^3. Tumor weight was calculated using an electronic weighing machine.

The rechallenge study: To evaluate whether Combo treatment exerted specific and long-term therapeutic effects, we performed a rechallenge assay. Mice were re-challenged with 3×10^5 CT26 murine colon cancer cells in the right lower flank or 2×10^5 4T1 murine breast cancer cells inoculated in the left breast fat pad in the left lower

flank without any subsequent treatment (on day 85 since the original tumor implanted in the Combo group or healthy mice of the same age) (Figure 5B). Thereafter, tumor volume was recorded continuously for 17 days.

The 4T1 murine breast cancer lung metastasis study: Six-to-eight-week-old female BALB/c mice were inoculated with 2×10^5 4T1 murine breast cancer cells in the right lower breast pad on day 0. On day 5, 1×10^5 4T1-luc murine breast cancer cells were intravenously injected to mimic the breast cancer lung metastasis. The treatment was started when the tumor volume in breast pad was around 50-100 mm^3. The luciferase images were taken on days 13, 16, and 19. The intensity of luciferin signal in mouse chest were measured using IVIS Series *In Vivo* Imaging Systems (PerkinElmer, USA). Mice were sacrificed on day 20 and their lungs were harvested and stored in Bouin's buffer (RS 4140, G-CLONE).

$CD4^+/CD8^+$ T lymphocyte or macrophage depletion assay: Six-week-old male BALB/c mice were inoculated with 3×10^5 CT26 murine colon cancer cells in the right upper flank on day 0. $CD8^+$ T, $CD4^+$ T, or macrophage depletion was performed by intraperitoneally injecting with anti-mouse CD8A (200 μg/100 μL/mouse/*i.p.*; clone 53-6.7; rat IgG2a; Bio X Cell)/ Isotype control (200 μg/100 μL/mouse/*i.p.*; clone 2A3; rat IgG2a; Bio X Cell) or CD4 (200 μg/100 μL/mouse/*i.p.*; clone YTS191; rat IgG2b; Bio X Cell)/ Isotype control (200 μg/100 μL/mouse/*i.p.*; clone LTF-2; Rat IgG 2b; Bio X Cell) or clodronate liposome (1 mg/200 μL/mouse/*i.p.*; Yeasen)/PBS liposome (1 mg/200 μL /mouse/*i.p.*; Yeasen) twice a week before Combo treatment began. PD-1

mAb (200 μg/100 μL/mouse/*i.p.*, clone BE0146, Bio X Cell) and GDNPs (200 μg/100 μL/mouse/*i.p.*) were administered every two days from day 8 for 5 times in total. Mice were sacrificed on day 21 and the tumor weight was calculated by an electronic weighing machine.

CCL5 and CXCL9 ***in vivo*** neutralization assay: Six-week-old male BALB/c mice were inoculated with 3×10^5 CT26 murine colon cancer cells in the right upper flank on day 0. $CD8^+$ T, $CD4^+$ T, or macrophage depletion was performed by intraperitoneally injecting with anti-mouse CCL5 (50 μg/100 μL/mouse/*i.p.*; clone 53405; rat IgG2a; R&D)/Isotype control (50 μg/100 μL/mouse/*i.p.*; Catalog: MAB006; rat IgG2a; R&D) or anti-mouse CXCL9 (100 μg/100 μL/mouse/*i.p.*; clone MIG-2F5.5; Armenian Hamster IgG κ; Bio X Cell)/ Isotype control (100 μg/100 μL/mouse/*i.p.*; Catalog: BE0091; Armenian Hamster IgG; Bio X Cell) twice a week after Combo treatment began. PD-1 mAb (200 μg/100 μL/mouse/*i.p.*, clone BE0146, Bio X Cell) and GDNPs (200 μg/100 μL/mouse/*i.p.*) were administered every two days from day 8 for 5 times in total. Mice were sacrificed on day 21 and the tumor weight was calculated by an electronic weighing machine.

GDNPs preparation

GDNPs were isolated from fresh *Panax ginseng C. A. Mey* root and prepared as previously published protocol.[21] The Bicinchoninic Acid Kit (Beyotime, China) was used to better quantify the GDNPs concentration. GDNPs measurement were performed using Nanoparticle Tracking Analyses NS3000 with NanoSight software.

For Transmission electron microscope image, 10 μL purified GDNPs was deposited onto the surface of formvar-coated copper grids, followed by incubation with 1% uranyl acetate for 15s. The samples were left to dry at room temperature and observed using a HITACHI H-7650 electron microscope operated at 80 kV at a magnification of 20, 000×. A sensitive LC-MS method has been developed for determination of Ginsenoside Re in GDNPs. For quantitative analysis, the separation of the multi-components was carried out by using the Waters Quattro Micro (series 2695; Waters, USA) liquid chromatography equipped with a quaternary pump, an online vacuum degasser, an autosampler, a thermostatic column compartment. All data collected were analyzed and processed using the Masslynx (Waters, USA). Chromatographic separation was performed on an Agilent HC-C_{18} column (4.6 mm × 250 mm, 5 μm, Agilent, USA) using gradient elution of acetonitrile-0.1% formic acid in water with a flow rate of 0.4 ml/min. The mass spectrometer was run in electrospray ionization (ESI +) mode by using multiple reaction monitoring (MRM).

Flow cytometry analysis of immune cells in the TME, splenocytes and peripheral blood

Immune cells were isolated by using Percoll (17-0891-09. GE Healthcare) from tumor cell suspension. These cells were incubated with CD16/32 (clone 93, BioLegend) for 15 min on ice and then were stained with various combinations of following fluorochrome-conjugated antibody at the appropriate dilutions for 30 min on ice, namely, CD3-APC/Cy7 (clone 145-2C11, BioLegend), CD8a-phycoerythrin (PE; clone

53-6.7, BioLegend), CD45-fluorescein isothiocyanate (FITC; clone 30-F11, BioLegend), CD11b-APC/Cy7 (clone M1/70, BioLegend), F4/80-PE/Cy7 (clone BM8, BioLegend), F4/80-BV421(clone BM8, BioLegend), CD8a-APC (clone 53-6.7, Biolegend), CD4-APC (clone GK1.5, BioLegend), CD4-PE/Cy7 (clone GK1.5 BioLegend), FVD506 (eflour 506, Invitrogen), CD45-BV510 (clone 30-F11, BioLegend), TIM3-PE (clone 5D12, BD Pharmingen), ICOS-PE/Cy7 (clone 7E.17G9, Invitrogen), PD-1-APC (clone 29F-1A12, BioLegend).

For T cell derived anti-tumor cytokines, 2×10^6 splenocytes or TILs were incubated in RPIM 1640 with Cell Stimulation Cocktail Plus Protein Transport Inhibitors (500×) for 6 h. Then cells were stained with surface markers and fixed and permeabilized using Fixation/Permeabilization kit (00-5123-43, 00-5223-56, Invitrogen), IFN-γ-PE/Cy7 (clone XMG1.2 BioLegend), granzyme B-FITC (clone NGZB, BioLegend), TNF-α-BB700 (clone MP6-XT22, BD Horizon) were diluent in Permeabilization buffer 10× (1:20) for 45 min.

Stained cells were analysed on a FACS Aria II Flow Cytometer, BD Biosciences) using BD FACSDiva software (BD Bioscience, USA) and data were processed using Flowjo Version 10 (BD Bioscience, USA).

Milliplex Luminex assay

Milliplex Luminex assay (Merk, Germany) was performed to examine the concentration of IL-2, IL-12 p40, and IL-12 p70 in mice plasma according to

manufacturer's instructions.

Reverse transcription PCR assay

Total RNA was isolated from 50,000 cells of M2-BMDM + GDNPs/PBS cultured with TRIzol reagent (Invitrogen) for 3min. The total RNA was reverse-transcribed using HiScript III RT SuperMix for qPCR (+gDNA wiper; category number R323-01; Vazyme Biotech), ChamQ Universal SYBR qPCR Master Mix (category number Q711-02; Vazyme Biotech). Primers were listed in the Supplemental Materials. Real-time PCR was performed using a 7500 Real-Time PCR System (Applied Biosystems, USA).

RNA-seq analyses

Total RNA of M2-BMDM + GDNPs/PBS was extracted using a TRIzol reagent kit (Invitrogen, Carlsbad, USA) according to the manufacturer's protocol. The RNA quality was examined using RNAse free agarose gel electrophoresis and processed using a 2100 Bioanalyzer Instrument (Agilent Technologies, USA). After total RNA was extracted, eukaryotic mRNA was enriched using Oligo(dT)beads, while prokaryotic mRNA was enriched by removing rRNA using Ribo-Zero TM Magnetic Kit (Epicenter, USA). Then, the enriched mRNA was fragmented using fragmentation buffer and reverse transcribed into cDNA with random primers. The second-strand cDNA was synthesized using DNA polymerase I, RNase H, dNTP and buffer. Then the cDNA fragments were purified with a QiaQuick PCR extraction kit (Qiagen, Netherlands), end repaired, poly(A) added, and ligated to Illumina sequencing adapters.

The ligation products were selected by size using agarose gel electrophoresis, PCR amplified, and sequenced using Illumina HiSeq2500 by Gene Denovo Biotechnology (Guangzhou, China).

Immunohistochemistry

Fresh organs such as heart, liver, spleen, lung, and kidney were fixed. Hematoxylin-eosin staining was performed to analyze microscopic pathological changes in murine main organs under Combo treatment by an optical microscope (Olympus, Japan). Fresh tumor samples were fixed with 4% paraformaldehyde for several days and embedded in paraffin, sectioned into 5-μm-thick sections and observed using a Leica RM 2235 (Leica, Germany) after being mounted on adhesive glass slides. BSA (Service Bio, G50001), and CD8 (GB13429, Service, 1:200) were used for staining to evaluate the infiltration of CTLs in tumors.

Immunofluorescent

For immunofluorescence, BMDMs on the microscope cover glass were fixed in ice-cold 4% paraformaldehyde. Sections were washed thrice with PBS for 5 min and mounted using ProLong Gold Antifade Mountant with DAPI (4′,6-diamidino-2-phenylindole; Thermo Fisher Scientific, USA) and imaged using 60× magnification with an Olympus FV10i confocal microscope (Olympus, Japan). The resultant digital images were analysed using the Olympus FluoView software version 4.0b. Images of three nonoverlapping optical fields covering the tumor sections surface were captured.

Image analysis was performed in ImageJ with the area measurement application or manual counting.

For OCT mounted CT26 murine colon tumor tissue sections, sliced samples were fixed in ice-cold 4% paraformaldehyde, after been incubated with 5% BSA, they were incubated with CD3-PE, CD8-APC overnight in 4 ℃. Following steps were same to BMDMs on the microscope cover glass.

Bioinformatic analysis

Correlation analysis between gene transcriptomes, such as CXCR3 and CCL9, CCR5 and CCL5 in COAD and BRCA patients in TCGA by using TIMER2.0 (http://timer.cistrome.org/).

Statistical analysis

The results are expressed as the mean ± standard error of mean. All data were analyzed using GraphPad Prism 7.0 (GraphPad Software, USA) by unpaired Student's t test, one-way or two-way analysis of variance (ANOVA), and log-rank (Mantel-Cox) test. $p < 0.05$ was considered statistically significant (* $p < 0.05$, ** $p < 0.01$, *** $p < 0.001$, **** $p < 0.0001$)

Supplementary Figures

Supplementary Figure 1

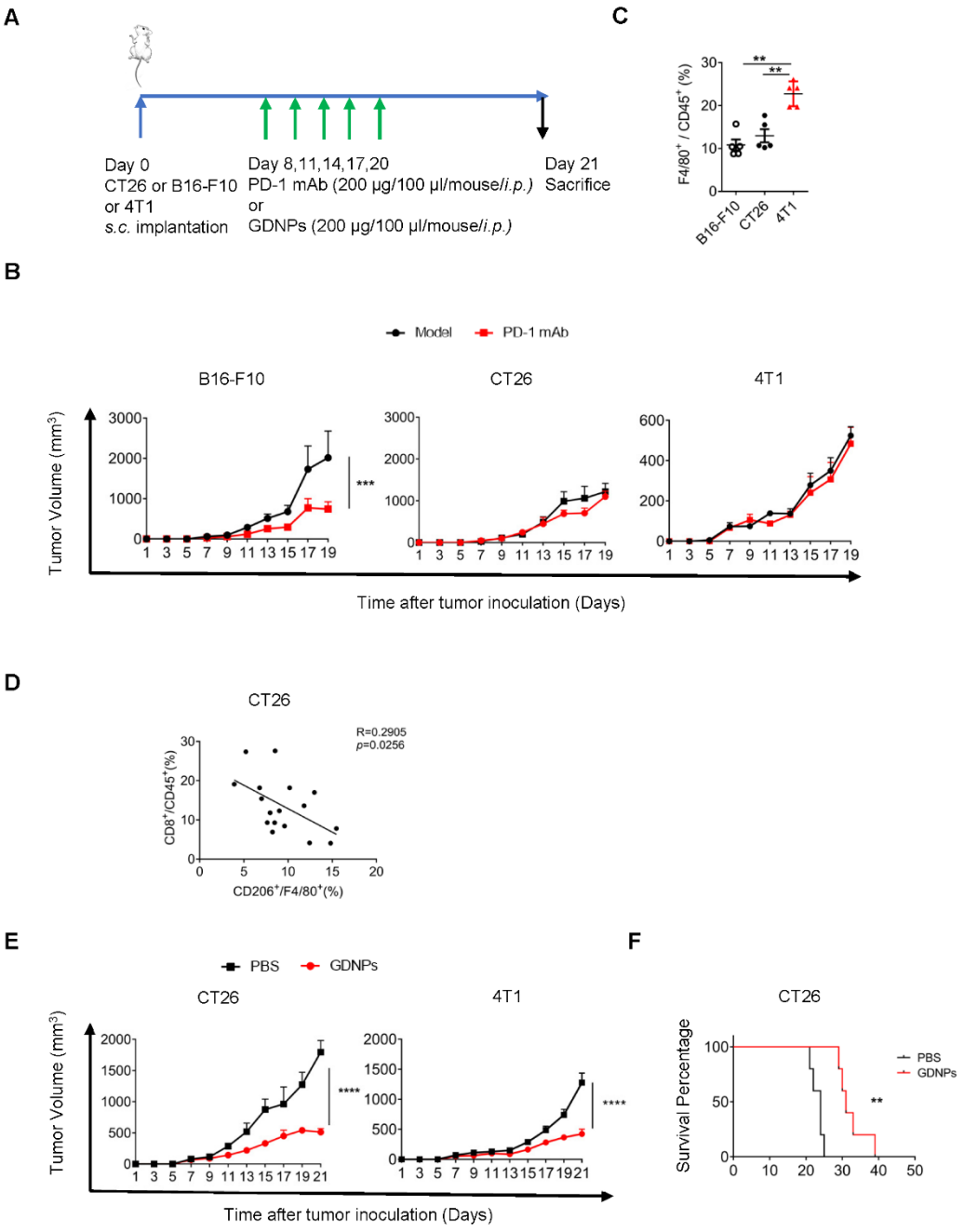

Figure S1. PD-1 mAb and GDNPs independent therapy in three tumor bearing mouse models. (A) Schematic of B16-F10 murine melanoma, CT26 murine colon

tumor, 4T1 murine breast tumor three mouse models under GDNPs/PD-1 Ab/Vehicle treatment regimen assay. (B) Tumor volume of B16-F10, CT26, 4T1 three murine tumor models under PD-1 mAb/Vehicle treatment. (n = 5 for each group, **p < 0.01) (C) Ratio of $F4/80^+/CD45^+$ in tumor immune microenvironment for B16-F10 melanoma, 4T1 breast cancer, CT26 colon cancer three murine tumor models (n = 5 for each group, ***p < 0.001). (D) Correlation analyses between ratio of $CD8^+/CD45^+$ and $CD206^+/F4/80^+$ for CT26 murine colon tumor model under GDNPs/Vehicle treatment. (for CT26 murine colon tumor model: n = 17, p = 0.0256, R = 0.2905) (E) Tumor volume of CT26 murine colon cancer, 4T1 murine breast cancer two murine models under GDNPs/PBS treatment. (n = 4 for each group, ****p < 0.0001) (F) Survival curve of mice treated with GDNPs or Vehicle controls. (n = 5 for each group, **p < 0.01) Data are presented as mean ± SEM and analyzed using student t test, Two-way ANOVA and Mantel-Cox test.

Supplementary Figure 2

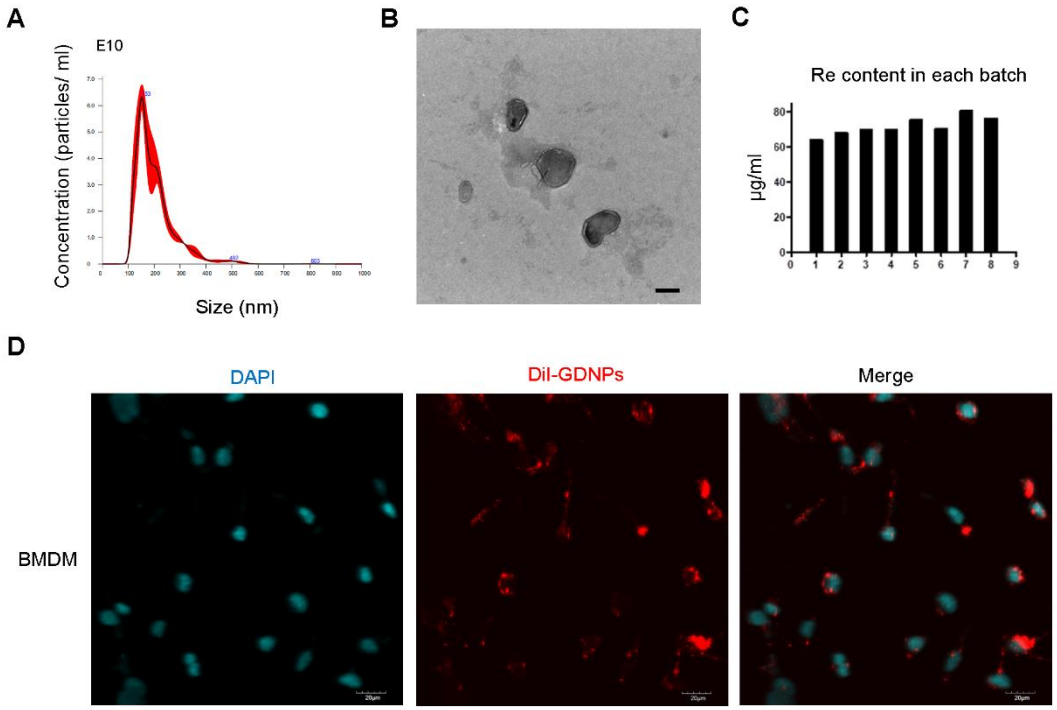

Figure S2. Characterization of ginseng-derived nanoparticles (GDNPs) prepared from fresh ginseng roots. (A) GDNPs were characterized by nanoparticle tracking system (NTA). (B) GDNPs from sucrose density gradient (45%) were characterized by transmission electron microscopy (TEM) (Scale bar = 200 nm). (C) Re ginsenoside content in each batch of GDNPs performed by HPLC-MS. (D) Immunofluorescent images for DiI-labelled GDNPs cocultured with BMDM (10 μg/ml). BMDMs were incubated with DiI-labelled GDNPs for 12 h. (scale bar = 20 μm)

Supplementary Figure 3

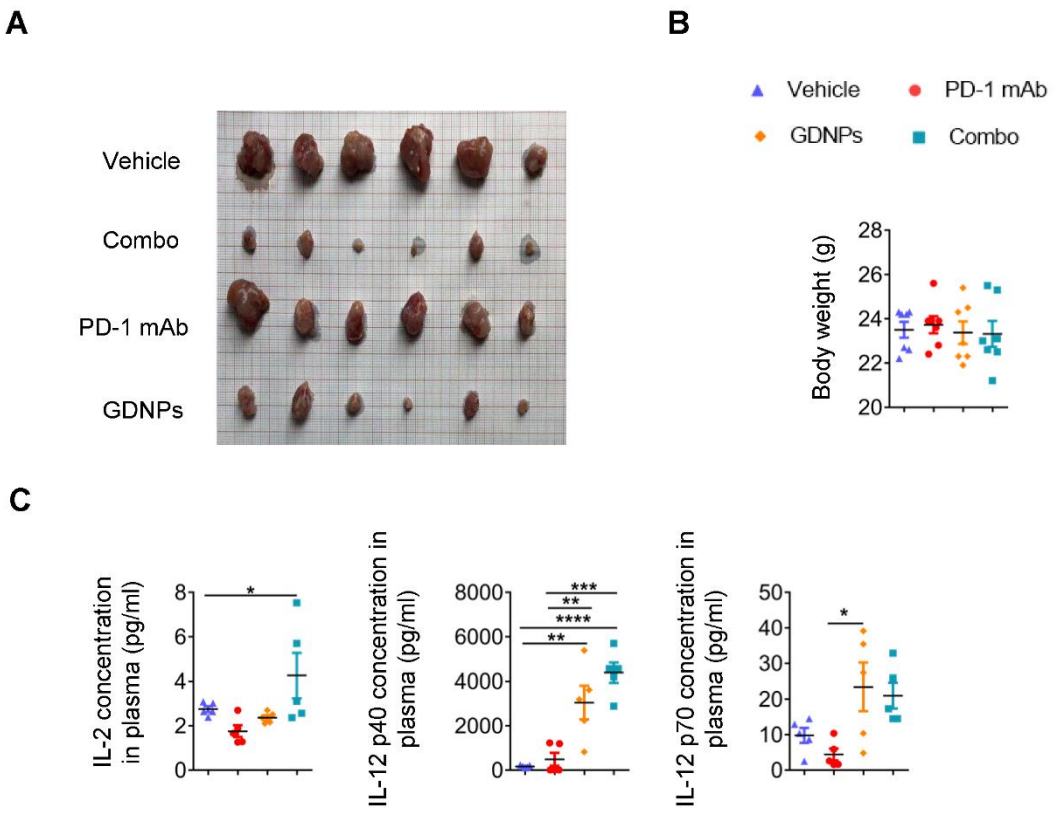

Figure S3. GDNPs combined with PD-1 mAb depresses CT26 murine colon tumor progression. (A) Tumor pictures for Vehicle, PD-1 mAb, GDNPs, Combo treatment (*n* = 6 for each group). (B) Body wight of CT26 tumor bearing mice under Vehicle, PD-1 mAb, GDNPs, and Combo treatment on day 21 before sacrifice. (n = 7 for each group) (C) IL-2, IL-12 p40, IL-12 p70 concentration in mice plasma by Milliplex Luminex assay. (n = 5 for each group, *p < 0.05, **p <0.01, ***p < 0.001, ****p < 0.0001). Data are presented as mean ± SEM and analyzed using One-way ANOVA.

Supplementary Figure 4

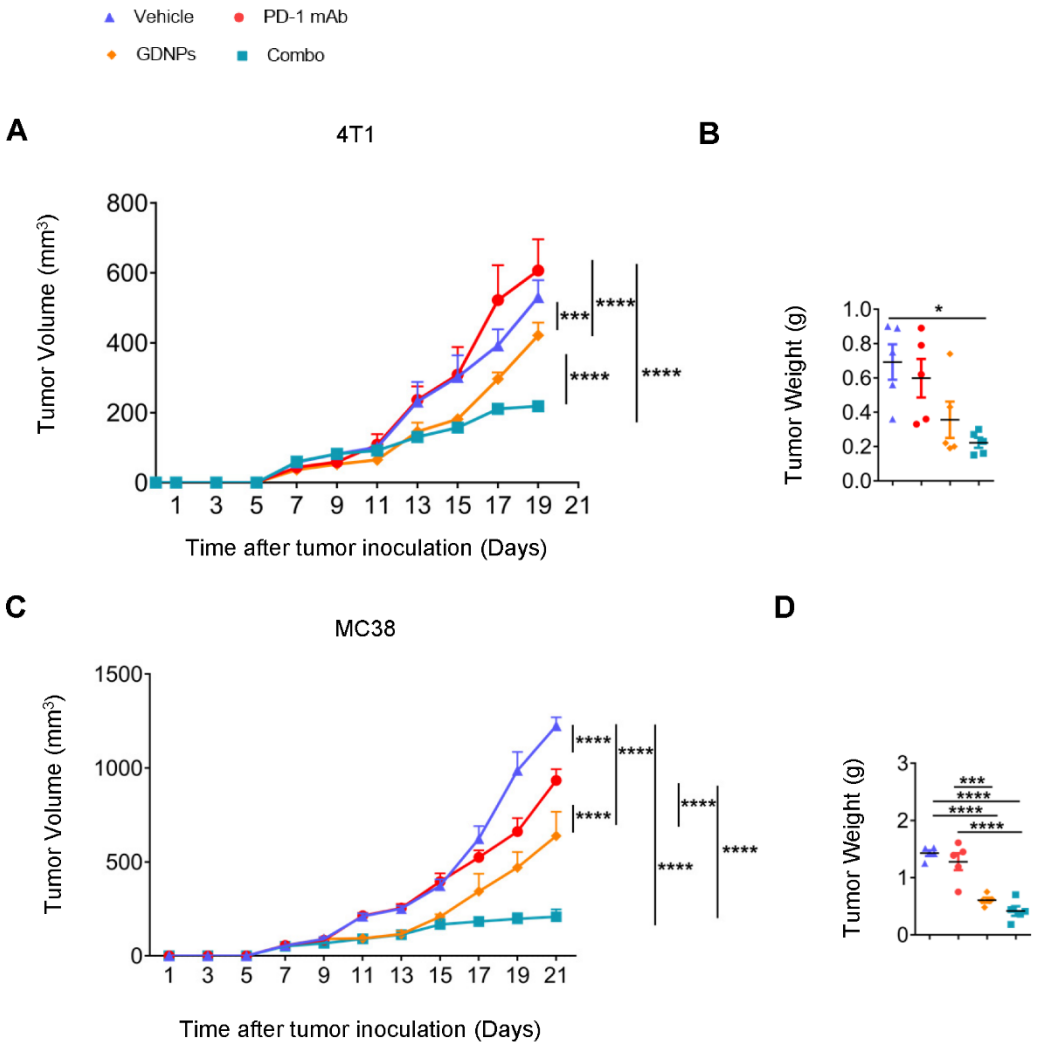

Figure S4. GDNPs combined with PD-1 mAb depresses 4T1 and MC38 murine tumor progression. (A) Tumor volume and (B) Day 21 Tumor weight for 4T1 murine breast cancer mouse model (n = 5 for each group, *p < 0.05, ****p < 0.0001). (C) Tumor volume and (D) Day 21 Tumor weight for MC38 murine colon tumor model (n = 5 for each group, ****p < 0.0001). Data are presented as mean ± SEM. Analyzed by One-way ANOVA or Two-way ANOVA.

Supplementary Figure 5

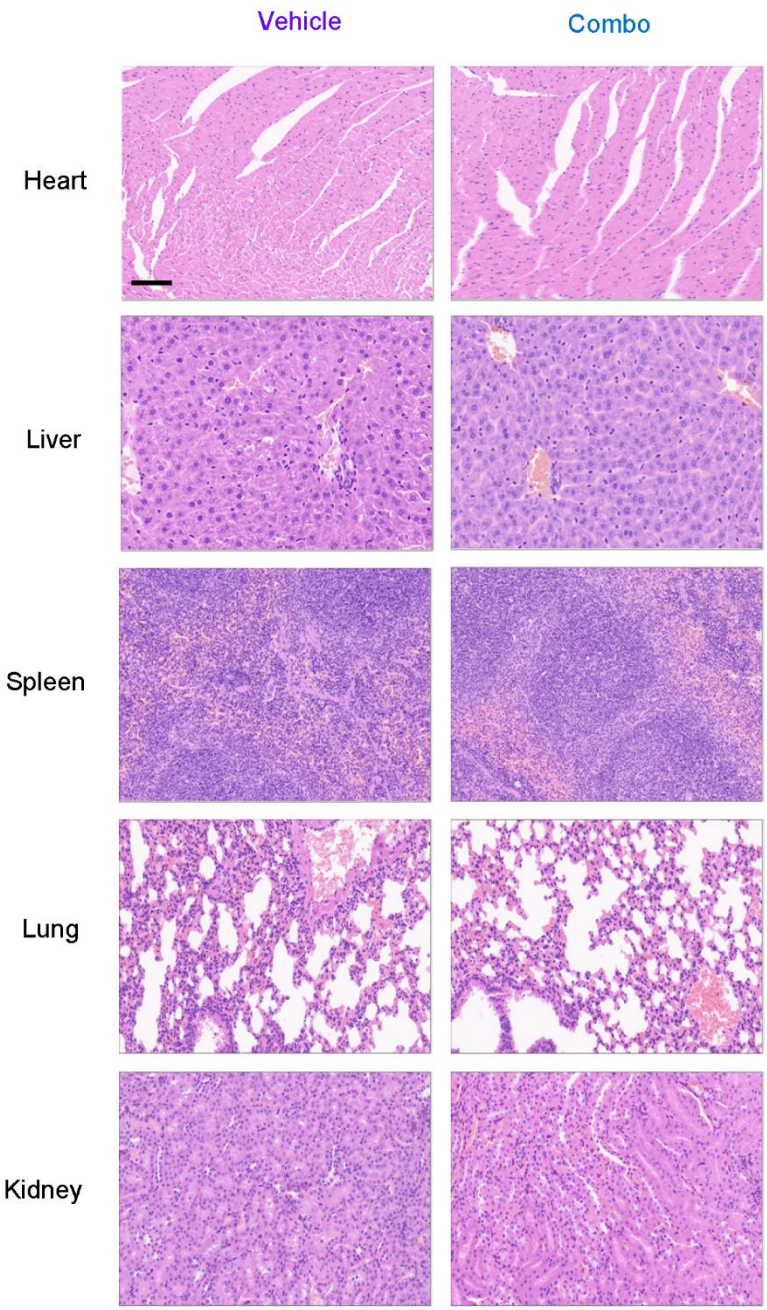

Figure S5. Safety evaluation assay. Analyses of microscopic pathological changes in murine main organs. Representative picture for HE staining for heart, liver, spleen, lung, kidney in Vehicle or Combo treatment group. (Scale bar = 50 μm).

Supplementary Figure 6

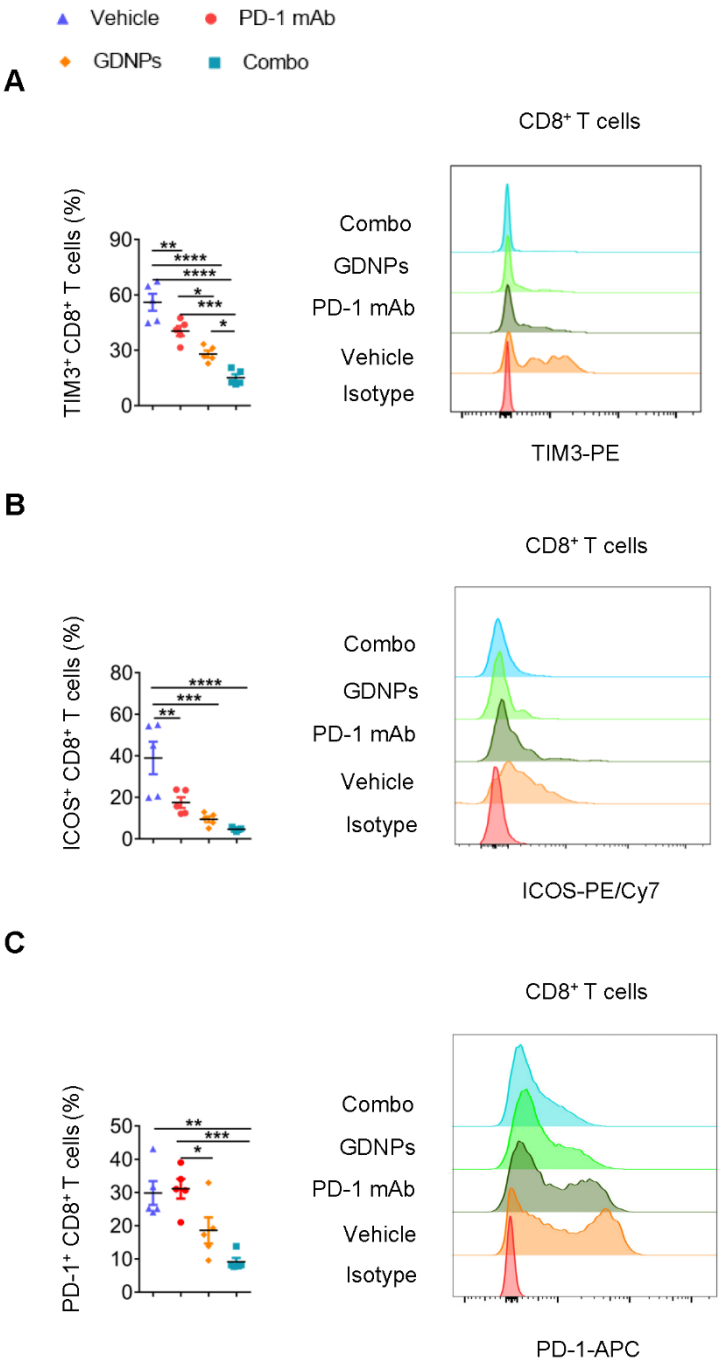

Figure S6. GDNPs combined with PD-1 mAb decreases immune checkpoint expression in T cell in CT26 murine colon tumor bearing mice. Fractions of (A) $TIM3^+$, (B) $ICOS^+$, (C) $PD\text{-}1^+$ in $CD8^+$ T cells and the representative flowcytometry

pictures in Vehicle, PD-1 mAb, GDNPs, and Combo groups. Data are presented as mean ± SEM. n = 5 for each group, *p < 0.05, **p < 0.01, ***p <0.001, ****p < 0.0001. Analyzed by One-way ANOVA.

Supplementary Figure 7

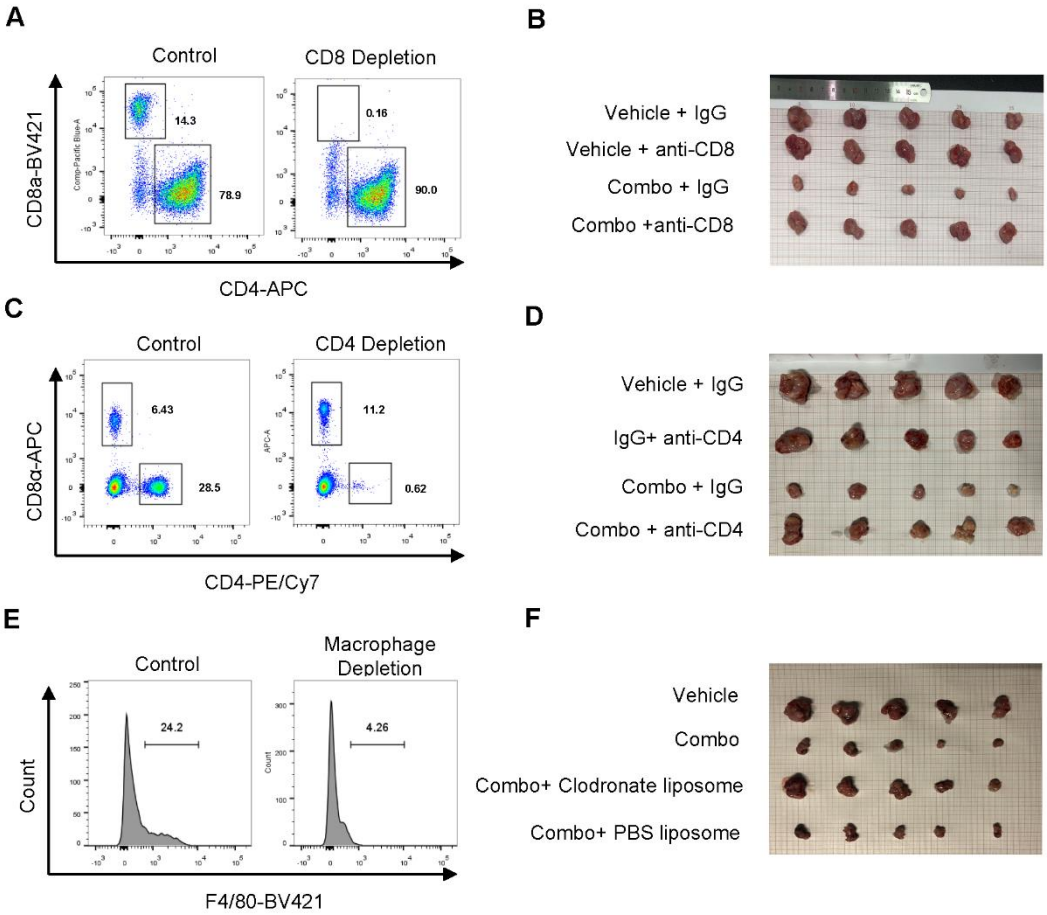

Figure S7. CD4$^+$, CD8$^+$ and macrophage *in vivo* depletion in CT26 murine colon tumor bearing mice. (A) Representative flow cytometric picture for CD8$^+$ T cell depletion verification in peripheral blood. (B) Tumor pictures for Vehicle + IgG, Combo + IgG, Vehicle + anti-CD8, Combo + anti-CD8. (C) Representative flow cytometric picture for CD4$^+$ T cell depletion verification in peripheral blood. (D) Tumor pictures for Vehicle + IgG, Combo + IgG, Vehicle + anti-CD4, Combo + anti-CD4. (E) Representative flow cytometric picture for macrophage depletion verification in peripheral blood. (F) Tumor pictures for Vehicle, Combo, Combo + Clodronate liposome, Combo + PBS liposome.

Supplementary Figure 8

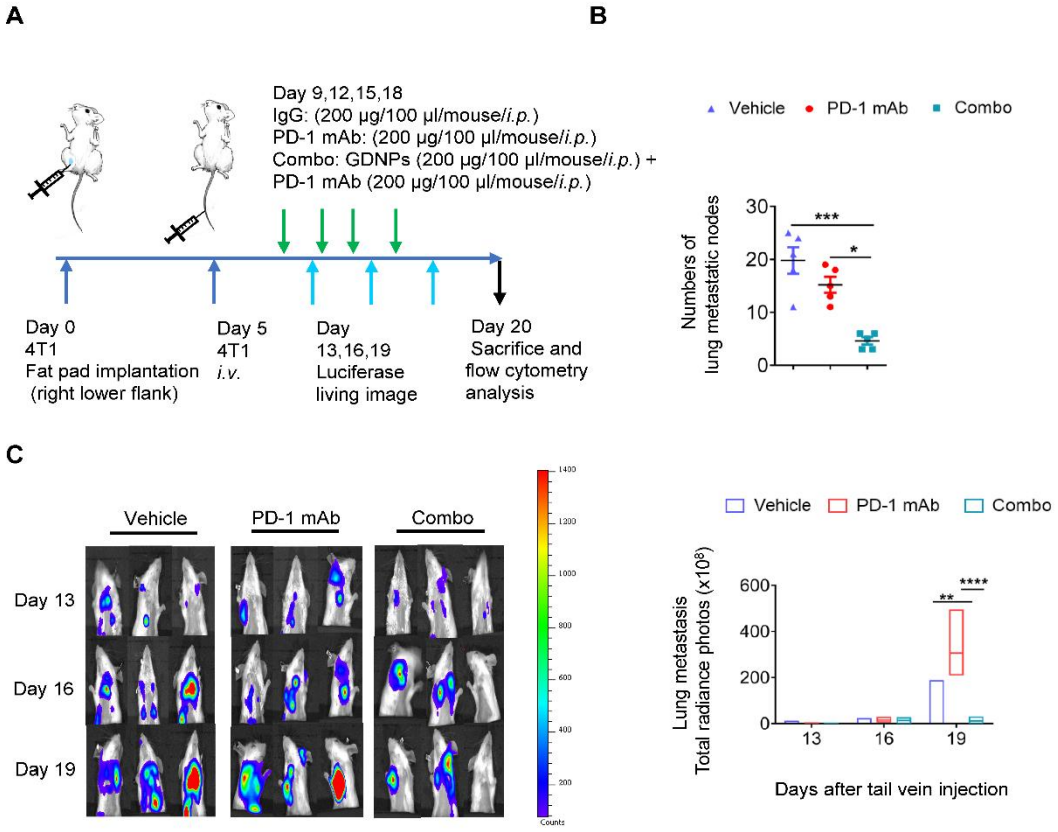

Figure S8. GDNPs combined with PD-1 mAb effectively inhibits 4T1 murine breast cancer lung metastasis. (A) Schematic diagram and administration methods for 4T1 murine breast cancer lung metastasis. (B) Quantification of 4T1 murine lung metastatic nodes in Vehicle, PD-1 mAb, and Combo groups ($n = 5$ per group, $^{*}p < 0.05$, $^{***}p < 0.001$). (C) Luciferase bioluminescent images of 4T1-Luc murine breast cancer lung metastasis in Vehicle, PD-1 mAb, and Combo groups. Results were calculated from three independent experiments. ($n = 3$ per group, $^{**}p < 0.01$, $^{****}p < 0.0001$) Data are presented as mean ± SEM. Analyzed by One-way ANOVA.

Supplementary Figure 9

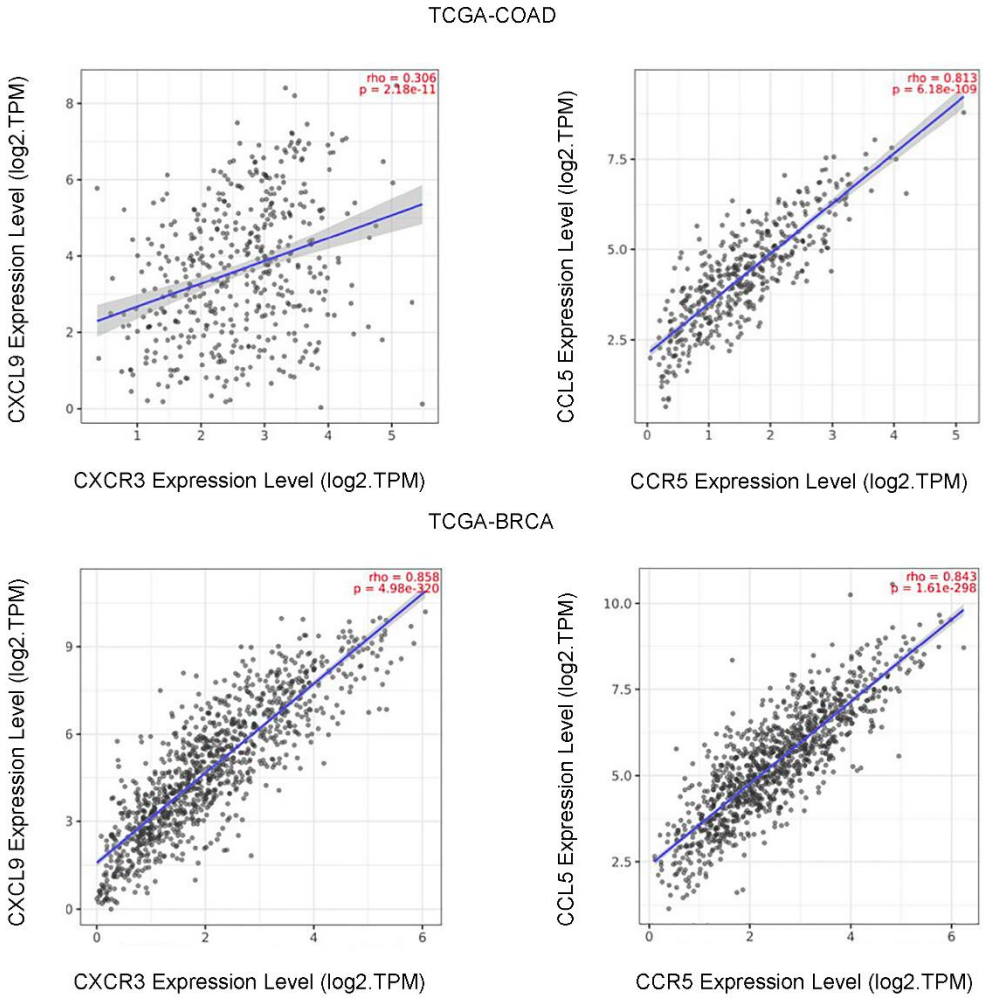

Figure S9. Correlation analyses between gene transcriptomes, such as CXCR3 and CCL9, CCR5 and CCL5 in COAD and BRCA patients in TCGA by using TIMER2.0 (http://timer.cistrome.org/).

Supplementary Figure 10

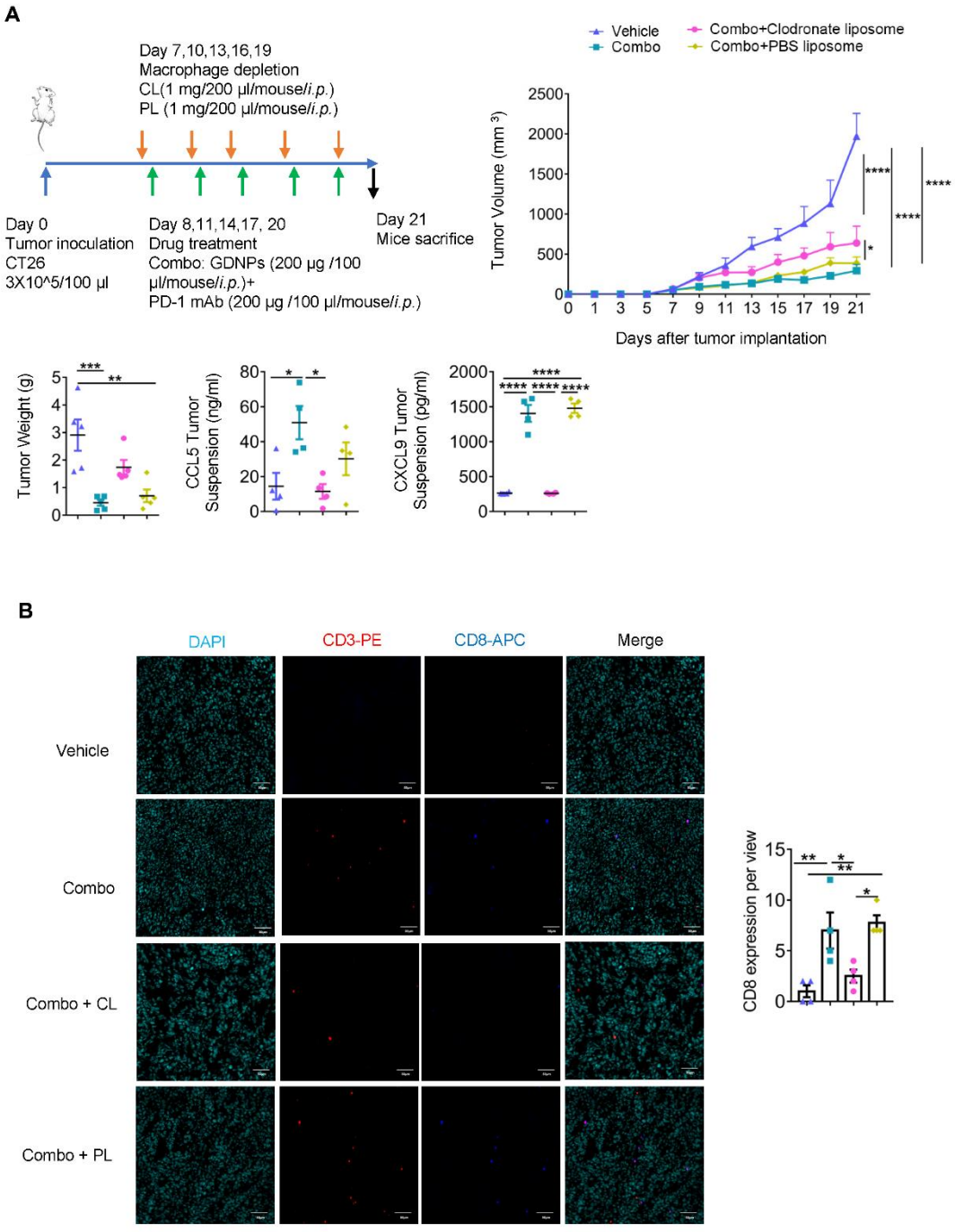

Figure S10. GDNPs activated macrophage recruited CD8$^+$ T lymphocytes into TME in CT26 murine colon tumor model. (A) Paradigm of tumor implantation, macrophage depletion assay by clodronate liposome (CL) or negative control PBS liposome (PL), drug treatment time schedule in CT26 murine colon tumor model.

Tumor volume and tumor weight for Combo, Combo + CL, Combo + PL, Vehicle four groups. CXCL9 and CCL5 concentration in tumor suspension in the four groups ($n = 5$ per group, $^{*}p < 0.05$, $^{**}p < 0.01$, $^{***}p < 0.001$, $^{****}p < 0.0001$). (B) Immunofluorescent staining of tumor sections in Combo, Combo + CL, Combo + PL, Vehicle groups ($n = 4$ per group, $^{*}p < 0.05$, $^{**}p < 0.01$). Data are presented as mean ± SEM. Analyzed by One-way ANOVA and Two-way AVONA.

Supplementary Figure 11

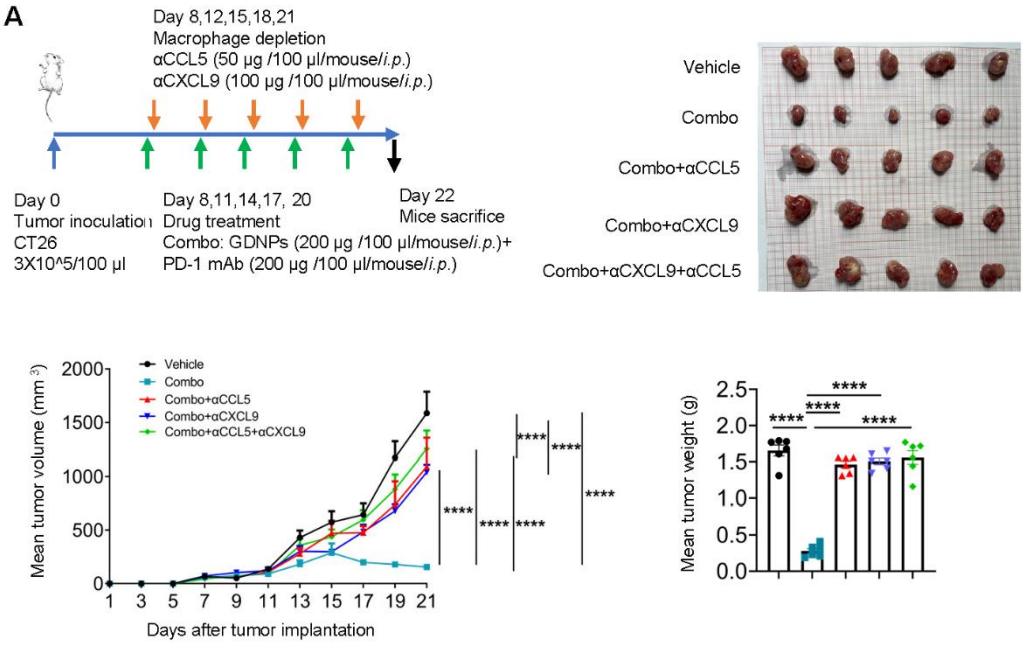

Figure S11. CCL5 and CXCL9 neutronization in CT26 murine colon model. (A) The time schedule, tumor picture, mean tumor volumes and tumor weight for chemokines *in vivo* neutralization assay (n = 5~6, Two-way ANOVA or One-way ANOVA).

Supplementary Figure 12

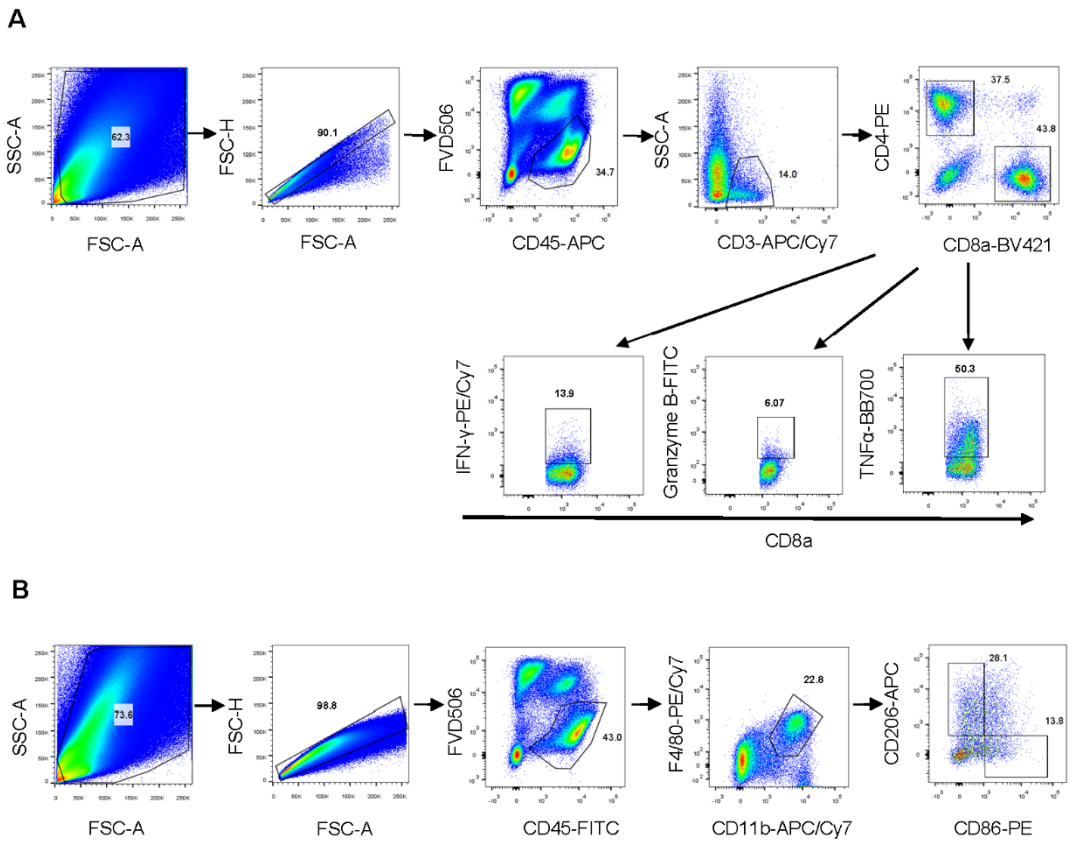

Figure S12. Flow cytometry gating strategy for tumor infiltrated (A)T lymphocytes and (B) macrophage polarization.